Cross-pathway integration of cAMP signals through cGMP and calcium-regulated phosphodiesterases in mouse striatal cholinergic interneurons

Ségolène Bompierre, Yelyzaveta Byelyayeva, Elia Mota, Marion Lefevre, Anna Pumo, Jan Kehler, Liliana R V Castro, Pierre Vincent

Received: 5 February 2024 | Revised: 4 September 2024 | Accepted: 21 October 2024

DOI: 10.1111/bph.17400

RESEARCH ARTICLE

Cross-pathway integration of cAMP signals through cGMP and calcium-regulated phosphodiesterases in mouse striatal cholinergic interneurons

Ségolène Bompierre[1] | Yelyzaveta Byelyayeva[1] | Elia Mota[1] | Marion Lefevre[1] | Anna Pumo[1] | Jan Kehler[2] | Liliana R. V. Castro[1] | Pierre Vincent[1,3]

[1]CNRS, Biological Adaptation and Ageing, Sorbonne Université, Paris, France

[2]H. Lundbeck A/S, Valby, Denmark

[3]IGF, University of Montpellier, CNRS, INSERM, Montpellier, France

Correspondence
Pierre Vincent, IGF, University of Montpellier, CNRS, INSERM, Montpellier, France.
Email: pierre.vincent@cnrs.fr

Funding information
Agence Nationale de la Recherche, Grant/Award Number: ANR-11-IDEX-0004-02; Association France Parkinson

Abstract

Background and Purpose: Acetylcholine plays a key role in striatal function. Firing properties of striatal cholinergic interneurons depend on intracellular cAMP through the regulation of I_h currents. Yet, the dynamics of cyclic nucleotide signalling in these neurons have remained elusive.

Experimental approach: We used highly selective FRET biosensors and pharmacological compounds to analyse the functional contribution of phosphodiesterases in striatal cholinergic interneurons in mouse brain slices.

Key Results: PDE1A, PDE3A and PDE4 appear as the main controllers of cAMP levels in striatal cholinergic interneurons. The calcium signal elicited through NMDA or metabotropic glutamate receptors activates PDE1A, which degrades both cAMP and cGMP. Interestingly, the nitric oxide/cGMP pathway amplifies cAMP signalling via PDE3A inhibition—a mechanism hitherto unexplored in a neuronal context.

Conclusions and Implications: The expression pattern of specific PDE enzymes in striatal cholinergic interneurons, by integrating diverse intracellular pathways, can adjust cAMP responses bidirectionally. These properties eventually allow striatal cholinergic interneurons to dynamically regulate their overall activity and modulate acetylcholine release. Remarkably, this effect is the opposite of the cGMP-induced inhibition of cAMP signals involving PDE2A in striatal medium-sized spiny neurons, which provides important insights for the understanding of signal integration in the striatum.

KEYWORDS
biosensor imaging, calcium, cAMP, cGMP, cholinergic interneurons, phosphodiesterases, striatum

Abbreviations: ChAT, Choline acetyltransferase; ChIN, cholinergic interneuron; DEANO, 2-[N,N-diethylamino]-diazenolate 2-oxide; MSN, medium-sized spiny neuron.

1 | INTRODUCTION

Basal ganglia play an important role in action selection, motor learning and reward, and striatal dysfunction is involved in various diseases such as Parkinson's, Huntington's and addiction. The vast majority of striatal neurons are **GABA**ergic projection neurons called medium-sized spiny neurons (MSN), while about 1% consists of cholinergic interneurons (ChINs). **Acetylcholine** works in concert with **dopamine** to ensure the temporal coordination of striatal circuitry and therefore defines a temporal window for learning (Krok et al., 2023; Mallet et al., 2019; Stocco, 2012). By synchronising MSN activity, ChINs are involved in changes and termination of movements (Gritton et al., 2019; Howe et al., 2019; Kondabolu et al., 2016) and behavioural learning (Mallet et al., 2019).

Regular spontaneous firing of ChINs maintains a cholinergic tone throughout the striatum, and this tonic firing is interspersed with burst–pause–rebound sequences coincident with phasic dopamine release (Aosaki et al., 2010). Electrophysiological studies revealed that ChIN activity is controlled by various neuromodulators involving the **cAMP** signalling pathway such as **noradrenaline** (via **β-adrenoceptors**) or dopamine (via **D_5 receptors**) (Aosaki et al., 1998; Pisani et al., 2003). ChINs show large I_h current, mainly mediated by the **HCN2 channel** (Notomi & Shigemoto, 2004; Zhao et al., 2016) which is under direct control by intracellular cAMP (Bennett et al., 2000; Deng et al., 2007; Kawaguchi, 1992; Santoro et al., 2000). The binding of cAMP to HCN channels shifts their activation curve, facilitating depolarisation and increasing the firing frequency. In spite of its considerable importance, the control of cAMP signalling pathway in ChIN remains poorly understood.

cAMP is a highly dynamic intracellular second messenger, whose concentration varies rapidly and is determined by production by **adenylyl cyclases** and degradation by **3',5'-cyclic nucleotide phosphodiesterases**. There are numerous isoforms of phosphodiesterases that vary, for example, in enzymatic specificity (cAMP and/or **cGMP**), Km and sub-cellular targeting (Chen et al., 2014; Chen et al., 2017; Muntean et al., 2018; Muntean et al., 2019; Neves et al., 2008). Moreover, their activity can be controlled by other second messengers, making these enzymes key hubs for cross-pathway regulations (Keravis & Lugnier, 2012). Each cell type expresses a precise subset of phosphodiesterases leading to distinct integrative properties.

Our objective was to determine which phosphodiesterases are functionally present in ChINs and how their presence might determine the integration of the cAMP signal. **PDE1A** is expressed in ChINs, as shown by immunocytochemical and single-cell transcriptomic analysis (Polli & Kincaid, 1994; Saunders et al., 2018). The PDE1 family degrades both cAMP and cGMP and is active only in the presence of **calcium-calmodulin** (Bender & Beavo, 2006), which suggests a potential link between calcium signals and the regulation of intracellular cyclic nucleotide levels. **PDE3A** mRNA is expressed in ChINs, as shown by single-cell RNA sequencing and by the punctate labelling in in situ hybridisation (Reinhardt & Bondy, 1996; Saunders et al., 2018). PDE3 has a sub-micromolar Km for cAMP and is inhibited by cGMP (Butt et al., 1992; Herget et al., 2008; Maurice, 2005; Maurice & Haslam, 1990; Shakur et al., 2001). The widely expressed **PDE4** family is also present in ChINs (Saunders et al., 2018). PDE4 does not degrade cGMP. While **PDE2A** and **PDE10A** are highly expressed in the striatum, they are below detection level in striatal ChINs (Sano et al., 2008; Saunders et al., 2018; Xie et al., 2006). Whether the predicted phosphodiesterases actually contribute to the regulation of cAMP in ChINs is unknown.

Genetically encoded FRET biosensors, which provide a direct measurement of intracellular signals in a physiologically relevant context, have revealed the importance of phosphodiesterases in the dynamic regulation of cyclic nucleotides. Using MSNs in striatal mouse brain slices, we have shown that **PDE1B** and PDE2A mediate the action of calcium or cGMP signals on cAMP (Betolngar et al., 2019; Polito et al., 2013). The aim of this study was to use a similar approach to monitor the functional contribution of the various phosphodiesterases in the regulation of cAMP levels in striatal ChINs and to explore how these phosphodiesterases might convey signals from **NO** and **glutamate** to the cAMP signalling pathway.

What is already known?

- Acetylcholine, released by cholinergic interneurons, plays an important functional role in the striatum.
- Cyclic nucleotides, under the control of phosphodiesterases, determine many critical neuronal properties including firing properties.

What this study adds?

- PDE1A, PDE3A and PDE4 are the main phosphodiesterase activities in cholinergic interneurons.
- PDE1A and PDE3A bridge glutamate/calcium and NO/cGMP pathways with cAMP signalling.

What is the clinical significance?

- PDE3, PDE1 or NO should be considered for evaluation as treatments for striatum-related diseases.

2 | METHODS

2.1 | Brain slice preparations

All animal care and experimental procedures complied with the Sorbonne University animal care committee regulations and were approved by the local Animal Ethics Committee (Charles Darwin,

project SA29). Animal studies are reported in compliance with the ARRIVE guidelines (Percie du Sert et al., 2020) and with the recommendations made by the *British Journal of Pharmacology* (Lilley et al., 2020).

These experiments were performed on mice, a widely-used animal model to study neurobiological processes. Neuronal survival and viral infection of brain slices were optimal in mice younger than 13 days, while the differentiation of neuronal types was already achieved. Brain slices were thus prepared from C57BL/6 J mice (Janvier Labs, Le Genest-Saint-Isle, France) aged from 7 to 12 days, weighing 3–6 g. Mice were kept in our animal facility under conditions of controlled temperature (22°C), humidity (55%) and light (12 h light/dark cycle), with free access to water and food. There is no indication of sex differences in the striatum at this age and both male and female mice were used in this study.

Mice were decapitated and the brain was quickly removed and immersed in an ice-cold solution of the following composition: 125 mM NaCl, 0.4 mM $CaCl_2$, 1 mM $MgCl_2$, 1.25 mM NaH_2PO_4, 26 mM $NaHCO_3$, 20 mM glucose, 2.5 mM KCl, 5 mM sodium pyruvate and 1 mM kynurenic acid, saturated with 5% CO_2 and 95% O_2. Coronal striatal brain slices of 300-µm thickness were cut with a VT1200S microtome (Leica). The slices were incubated in this solution for 30 min and then placed on a Millicell-CM membrane (Millipore) in culture medium (50% Minimum Essential Medium, 50% Hanks' Balanced Salt Solution, 5.5 g L^{-1} glucose, penicillin–streptomycin, Invitrogen). The cAMP biosensor Epac-S^{H150} (Polito et al., 2013), cGMP biosensor cyGNAL (Betolngar et al., 2019) and calcium biosensor Twitch-2B (Thestrup et al., 2014) were expressed using the Sindbis virus as vector (Ehrengruber et al., 1999). The viral vector was added on the brain slices ($\sim 5 \times 10^5$ particles per slice), and the infected slices were incubated overnight at 35°C under an atmosphere containing 5% CO_2. Before the experiment, slices were incubated for 30 min in the recording solution (125 mM NaCl, 2 mM $CaCl_2$, 1 mM $MgCl_2$, 1.25 mM NaH_2PO_4, 26 mM $NaHCO_3$, 20 mM glucose, 2.5 mM KCl and 5 mM sodium pyruvate saturated with 5% CO_2 and 95% O_2). Recordings were performed with a continuous perfusion of the same solution at 32°C.

2.2 | Biosensor imaging

Imaging was performed in slices from the dorso-medial part of the striatum. Wide-field images were obtained with an Olympus BX50WI or BX51WI upright microscope with a 40 × 0.8 numerical aperture water-immersion objective and an ORCA-AG camera (Hamamatsu). Images were acquired with iVision (Biovision, Exton, PA, USA). The excitation and dichroic filters were D436/20 and 455dcxt. Signals were acquired by alternating the emission filters, HQ480/40 for donor emission and D535/40 for acceptor emission, with a filter wheel (Sutter Instruments, Novato, CA, USA). The frequency of data acquisition was usually 1 image pair every 30 or 60 s but was increased to resolve transient responses. To increase the number of recorded neurons, up to three focal depths were recorded for each timepoint. Excitation power at the exit of the microscope objective was 400 to 1400 µW. Photorelease of **NMDA** from 'caged' precursor MNI-NMDA was performed using a high power 360-nm light-emitting diodes mounted on the epifluorescence port of the microscope, for 0.5 s duration with 14 mW power at the exit of the microscope objective. Filters were obtained from Chroma Technology and Semrock. LED light sources (420 nm with a 436 nm excitation filter and 360 nm) were purchased from Mightex (Toronto, Canada).

Wide-field imaging allowed for the separation of ChINs signal from MSNs, provided that the infection level was kept low and no fluorescence overlap between neighbouring neurons was observed. In a few cases, cells were excluded when basal ratio was elevated, when the response to maximal stimulation was lacking or when the neuronal morphology was altered (uneven cell contours). At the end of every biosensor imaging experiment, an image stack was acquired to ascertain the morphology of the recorded cells in three dimensions.

An application of **tetrodotoxin (TTX**; 200 nM) for 5 min preceded drug applications to stop any ongoing spontaneous activity; in some cases, this induced a decrease in Twitch-2B ratio, consistent with the ChIN exhibiting a tonic firing activity before TTX action.

2.3 | Data and statistical analysis

Images were analysed with a custom software, Ratioscope (DOI: 10.5281/ZENODO.11059482), written in the IGOR Pro environment (Wavemetrics, Lake Oswego, OR, USA) as described previously (Polito et al., 2014). No correction for bleed-through or direct excitation of the acceptor was applied. Biosensor activation level was quantified by ratiometric imaging: donor fluorescence divided by acceptor fluorescence for Epac-S^{H150} and cyGNAL, and acceptor divided by donor for Twitch-2B. The emission ratio was calculated for each pixel and displayed in pseudo-colour images, with the ratio value coded in hue and the fluorescence of the preparation coded in intensity. The ratio value varies between Rmin, the ratio in the absence of ligand, and Rmax, the ratio in the presence of saturating ligand. For the Epac-S^{H150} biosensor for cAMP, considering the low cAMP tone in ChIN (see further discussion), the basal ratio was assumed to be Rmin. Rmax was determined for each neuron by the final application of 13 µM **forskolin** and 200 µM **IBMX**, which is commonly accepted as a condition in which the biosensor is saturated with cAMP (Börner et al., 2011). For the cyGNAL biosensor for cGMP, baseline ratio was considered equal to Rmin (see below); Rmax was determined for each neuron by the final application of the NO donor, 2-[N,N-diethylamino]-diazenolate 2-oxide (DEANO; 10 µM) and IBMX (200 µM). For both biosensors, all ratio traces are normalised between Rmin = 0 and Rmax = 1 before calculating averages, and labelled 'fraction of maximal response'. For the Twitch-2B biosensor for calcium, the Rmax value was difficult to determine because common manipulations aiming at maximising intracellular calcium, such as NMDA, ionomycin or KCl applications, triggered ratio increases of inconsistent and unstable value. Calcium measurements are therefore presented as raw ratio values.

Biosensor concentration was estimated from the fluorescence intensity measured as follows. A vertical image stack was acquired at the end of each experiment. For each recorded neuron, the plane in the stack where the neuron showed the best contrast was selected. Because the whole region of interest encompasses some background or dimmer regions of the cell, the intensity was evaluated over the 20% brightest pixels within the region of interest in this plane of the stack. This value is corrected for camera offset, exposure duration, excitation power and shading correction, and expressed as counts per pixel per milliwatt of power excitation per second (c mW^{-1} $pixel^{-1}$ s^{-1}).

Ratiometric imaging can be used to determine absolute analyte concentrations, with ratio values following a Hill equation from Rmin to Rmax (Grynkiewicz et al., 1985). For averaged recordings with Epac-S^{H150}, an axis on the right presents cAMP concentration estimates based on these Rmin and Rmax value, a Hill equation with a Kd of 10 µM and a Hill coefficient of 0.77 (Klarenbeek et al., 2015; Polito et al., 2013). For averaged recordings with cyGNAL, an axis on the right presents cGMP concentration estimates based on these Rmin and Rmax value, a Hill equation with a Kd of 0.465 µM and a Hill coefficient of 0.8 (Betolngar et al., 2019).

Statistical tests were performed in accordance with the BJP's recommendations and requirements on experimental design and analysis (Curtis et al., 2022) with the same Ratioscope package using built-in Igor Pro functions. Brain slices were considered independent. Experimenters performed the experiments unblinded. One experiment is defined as one brain slice being used in a protocol such as that illustrated in Figure 2a. Only a single experiment was performed on a brain slice. While most experiments were performed with a single ChIN, if more than one was present in an experiment (up to 4), their responses were considered as 'technical replicates', averaged and counted as one measurement. Except for Figure 1, statistics were calculated per experiment (*n*) with at least five experiments; (*N*) indicates the total number of neurons per condition, that is, sample size including technical replicates; (*A*) indicates the number of animals used for preparing all the brain slices used per condition. No outlier was excluded in this study. The alpha level for statistical significance was 0.05. For some conditions, the Shapiro–Wilk test rejected the hypothesis of normal data distribution, and therefore, non-parametric statistics were used throughout this study. The median value is displayed on graphs and indicated in the figure legend. The Wilcoxon signed rank test was used to compare two measurements of paired data. The Friedman's rank test was used to determine an effect when more than two conditions were compared. The Wilcoxon–Mann–Whitney test was used to test whether the treatment increased the ratio value for unpaired data.

2.4 | Immunohistochemistry

After biosensor imaging, brain slices were fixed by overnight immersion in a 4% paraformaldehyde (PFA) in phosphate buffer (0.1 M, 4°C, pH 7.4). They were then stored at −20°C in a phosphate buffer containing 30% (*v*/*v*) glycerol and 30% (*v*/*v*) ethylene glycol, until they were processed for immunofluorescence. **Choline acetyltransferase (ChAT)** expression was detected with a freshly prepared goat polyclonal antibody (1:500; 4°C overnight, AB144p, RRID:AB_2079751, Merck) and revealed with the freshly prepared secondary antibody Alexa Fluor 647 donkey anti-goat IgG (1:500, RRID:AB_2340437, Jackson ImmunoResearch) imaged with F39-628 filter for excitation, F37-692 filter for emission and F38-661 dichroic mirror (Olympus). Following the incubation of the primary antibodies (4°C, overnight incubation), brain sections were rinsed and incubated with the secondary antibody for 2 h at room temperature. Floating slices were rinsed and images were acquired with a wide-field microscope.

2.5 | Materials

Solutions were prepared from powders purchased from Sigma-Aldrich (St Quentin-Fallavier, Isère, France). Tetrodotoxin (TTX) was from Latoxan (Valence, France). DEANO was from Bertin Technologie (Saint-Quentin-en-Yvelines, France). Other compounds and drugs were from Tocris Bio-Techne (Lille, France). All drugs with full name, abbreviation, target and usual concentration are presented in Table 1.

2.6 | Nomenclature of targets and ligands

Key protein targets and ligands in this article are hyperlinked to corresponding entries in http://www.guidetopharmacology.org and are permanently archived in the Concise Guide to PHARMACOLOGY 2021/22 (Alexander, Christopoulos et al., 2023; Alexander, Fabbro et al., 2023; Alexander, Mathie et al., 2023).

3 | RESULTS

3.1 | Identification of cholinergic interneurons in a brain slice

We used genetically encoded biosensors to explore intracellular signalling events in individual neurons in the context of brain slices from mouse pups. Sparse biosensor expression in neurons was obtained after overnight incubation of brain slices with the Sindbis viral vector as described previously (Polito et al., 2014). In the course of our previous studies on cAMP dynamics in MSNs, we were intrigued by the odd behaviour of a small fraction of neurons in the imaging field which showed small and slow cAMP responses to forskolin (13 µM, Figure 1a). We verified that the moderate size of the cAMP response to forskolin did not result from a buffering effect of excessive biosensor expression: the biosensor expression level was estimated for each neuron from the fluorescence intensity of the cell body (see Section 2.3). There was no correlation between the amplitude of the cAMP response in these neurons and the biosensor expression level (Figure 1b, middle), ruling out an artefactual effect of biosensor level on these neurons' responsiveness to forskolin. The response to

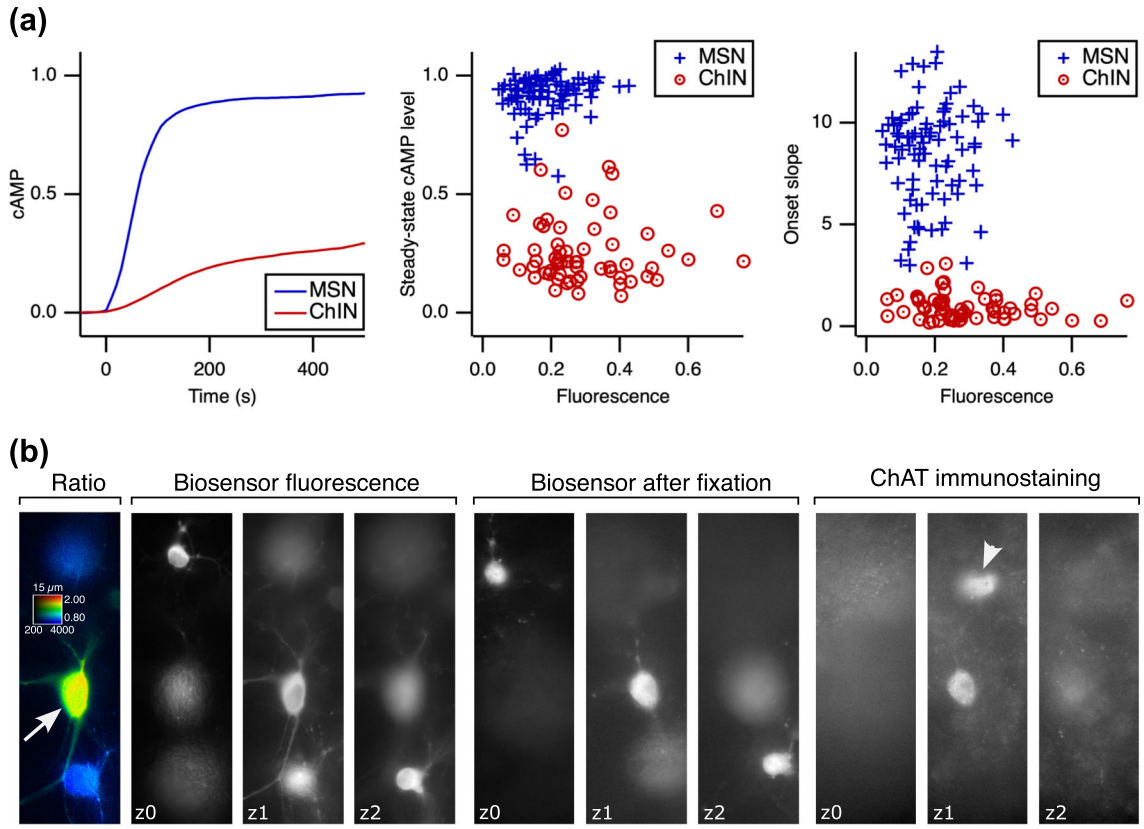

FIGURE 1 **Biosensor imaging in mouse brain slices and identification of striatal cholinergic interneurons (ChINs).** (a) cAMP response to forskolin in striatal ChINs and MSNs, recorded with the Epac-S^{H150} biosensor. Left: the responses to forskolin (13 µM) were averaged for each neuronal type, red for ChINs ($n = 47$ experiments, $N = 69$ individual neurons, $A = 21$ animals) and blue for MSNs ($n = 38$, $N = 105$, $A = 21$). The maximal cAMP response in forskolin and IBMX (200 µM) was used for normalisation. Biosensor fluorescence (in counts mW^{-1} $pixel^{-1}$ s^{-1}), used as an estimate of biosensor expression level, was measured on part of these neurons: 0.27 in ChINs ($N = 60$), significantly ($P<0.05$) larger than 0.19 in MSNs ($N = 87$). Steady-state cAMP level (middle graph): 0.22 for ChINs significantly different from 0.94 for MSNs; correlation coefficient for ChINs: $r = -0.04$. Onset slope (right graph) measured over 80 s: 0.82 in ChINs, significantly different from 8.66 in MSNs; correlation coefficient for ChINs: $r = -0.17$. (b) ChINs identification in brain slices. This brain slice was transduced for the expression of the Twitch-2B calcium biosensor. The pseudocolour image (left) displays the biosensor emission ratio in two MSNs and one ChIN (arrow). At the end of the recording, the slice was fixed and immunostained for choline acetyltransferase (ChAT).Three different focal planes (z0, z1 and z2) are represented in the images in grey levels. From left to right: biosensor fluorescence during the biosensor imaging session, after slice fixation with PFA and after ChAT immunostaining. The arrow indicates a ChIN; the other neurons are putative MSNs except for one additional ChIN revealed by ChAT that did not express the biosensor (arrowhead). Note the lack of bleed-through of biosensor fluorescence to the ChAT immunostaining channel.

forskolin also appeared much slower in these neurons than in MSNs (Figure 1a, right). The onset slope did not appear related to biosensor concentration, again arguing against a buffering effect of biosensor on cAMP signal. The morphology of these neurons was also quite distinct from that of the MSNs, with a cell body diameter of over 13 µM, an elongated cell body, an ovoid nucleus and wide proximal dendrites, suggesting they were cholinergic interneurons (ChINs; Kawaguchi, 1993; Tepper et al., 2010). This morphological identification was confirmed by immunohistochemical labelling of choline acetyltransferase (ChAT) after biosensor imaging experiments (Figure 1b). Eleven brain slices were fixed after the biosensor experiment and later processed for ChAT immunoreactivity. In these slices, 15 neurons were visually identified as ChINs during the biosensor recording session and all of these neurons showed a positive ChAT labelling.

3.2 | PDE3 and PDE4 control cAMP levels in ChIN at rest

Considering the attenuated cAMP responses in ChINs, our first objective was to identify which phosphodiesterases were involved in the negative control of cAMP levels. We performed wide-field microscopy, sometimes at several focal planes in the same location, to record more ChINs in the same experiment (Figure 2a, ChIN 0 and ChIN 1 on the first focal plane [z0 image] and ChIN 2 on the second focal plane [z1 image]). We first stimulated cAMP production with forskolin, which increased cAMP level moderately in ChINs, and then added the selective PDE3 inhibitor **cilostamide** (10 µM) which increased the ratio in ChINs to a higher steady-state level. Further addition of the selective PDE4 inhibitor **piclamilast** (1 µM) brought the ratio to a

TABLE 1 Drugs.

Full name	Abbreviation	Effect	Target	Concentration
Tetrodotoxin	TTX	Inh.	Voltage-activated sodium channels	0.2 μM
Forskolin	fsk	Act.	Adenylyl cyclases (except 9)	0.5–13 μM
Isobutylmethylxanthine	IBMX	Inh.	Phosphodiesterases (except 8 & 9)	200 μM
Lu AF64196		Inh.	PDE1	1–10 μM
PF-05180999		Inh.	PDE2A	1 μM
Cilostamide	cilo	Inh.	PDE3	10 μM
Piclamilast	picla	Inh.	PDE4	1 μM
Rolipram	roli	Inh.	PDE4	1 μM
Roflumilast		Inh.	PDE4	1 μM
TP-10		Inh.	PDE10A	0.1 μM
2-(N,N-diethylamino)-diazenolate 2-oxide	DEANO		NO donor	1–10 μM
ODQ		Inh.	Soluble G cyclase	20 μM
4-Methoxy-7-nitroindolinyl-caged-NMDA	MNI-NMDA	Act.	NMDA receptor	100 μM
3,5-DHPG	DHPG	Act.	Group 1 mGlu	50 μM
Quisqualate		Act.	AMPA and group 1 mGlu	1 μM
NBQX		Inh.	AMPA	1 μM
D-AP5		Inh.	NMDA	20 μM

Note: List of the drugs used in this study. Effect indicates inhibitor (inh.) or activator (act.).

higher level. The ratio was not further raised by the non-specific phosphodiesterase inhibitor IBMX (200 μM), indicating the saturation level of the biosensor by cAMP (Rmax). These experiments were repeated with similar results (Figure 2d, left). PDE3 thus contributes importantly to the regulation of cAMP level, and when this phosphodiesterase is inactivated pharmacologically, PDE4 remains to control cAMP level.

We then wondered whether this situation was similar when PDE4 is inhibited first while PDE3 is active. In a similar protocol, on top of forskolin stimulation, PDE4 was first inhibited with piclamilast, which induced an increase in cAMP level in ChINs (Figure 2b). PDE4 activity thus also contributes to the regulation of cAMP level reached upon forskolin application, even though PDE3 is present and active. Indeed, further application of cilostamide increased the ratio to Rmax, the level that was not raised by IBMX. This protocol was repeated with similar results (Figure 2d, second panel).

We explored the contribution of other phosphodiesterases that are expressed in the striatum. Because PDE2A regulates elevated cAMP levels, its activity was tested when adenylyl cyclases were activated and PDE3 was inhibited (Figure 2c). In the presence of forskolin and cilostamide, the ratio level in the presence of the selective PDE2A inhibitor **PF-05180999** (PF-05, 1 μM) was slightly increased compared to the previous steady-state level (Figure 2d, third panel). The amplitude of the response to PF-05 was however considerably smaller than the effect of piclamilast (Wilcoxon–Mann–Whitney test). PDE10A has a high affinity for cAMP, and we wanted to test its potential effect on lower cAMP levels, that is, in a condition in which PDE3 and PDE4 are active. The PDE10A inhibitor **TP-10** (100 nM) had no effect on the forskolin-induced steady-state cAMP level (Figure 2d, fourth panel), indicative of no PDE10A activity in ChINs.

We then wanted to determine whether ChINs displayed a tonic cAMP production. In the absence of forskolin, the combination of **rolipram** and cilostamide induced no significant ratio change in ChINs (Figure 2d, right), indicating that basal cAMP production in these conditions is negligible. This comes in stark contrast with the tonic cAMP production revealed in MSNs when inhibiting PDE10A (Polito et al., 2015).

Collectively, these experiments show that in striatal ChINs, when cAMP production is stimulated, cAMP levels remain low by the combined action of PDE3 and PDE4.

3.3 | The cGMP pathway increases cAMP levels through PDE3 inhibition

PDE3 degrades both cAMP and cGMP, but the Vmax of PDE3 for cGMP is very low and cGMP thus behaves in vitro as a competitive inhibitor of PDE3 activity towards cAMP hydrolysis (Shakur et al., 2001). Furthermore, a **PKG**-dependent phosphorylation site in PDE3A that negatively regulates PDE3A activity has been reported (Zemskov et al., 2021). We therefore pondered whether a cGMP signal, by inhibiting PDE3, could increase cAMP level. We used the NO donor compound DEANO which activates the **soluble guanylyl cyclase** and increases cGMP levels. After forskolin increased cAMP to a steady-state level, the application of DEANO (10 μM) produced a marked cAMP increase. This cAMP level was not further increased by the application of the PDE3 inhibitor cilostamide (Figure 3a and 3b, left panel). DEANO thus reproduces and occludes the effect of cilostamide. Conversely, when added on top of forskolin and cilostamide,

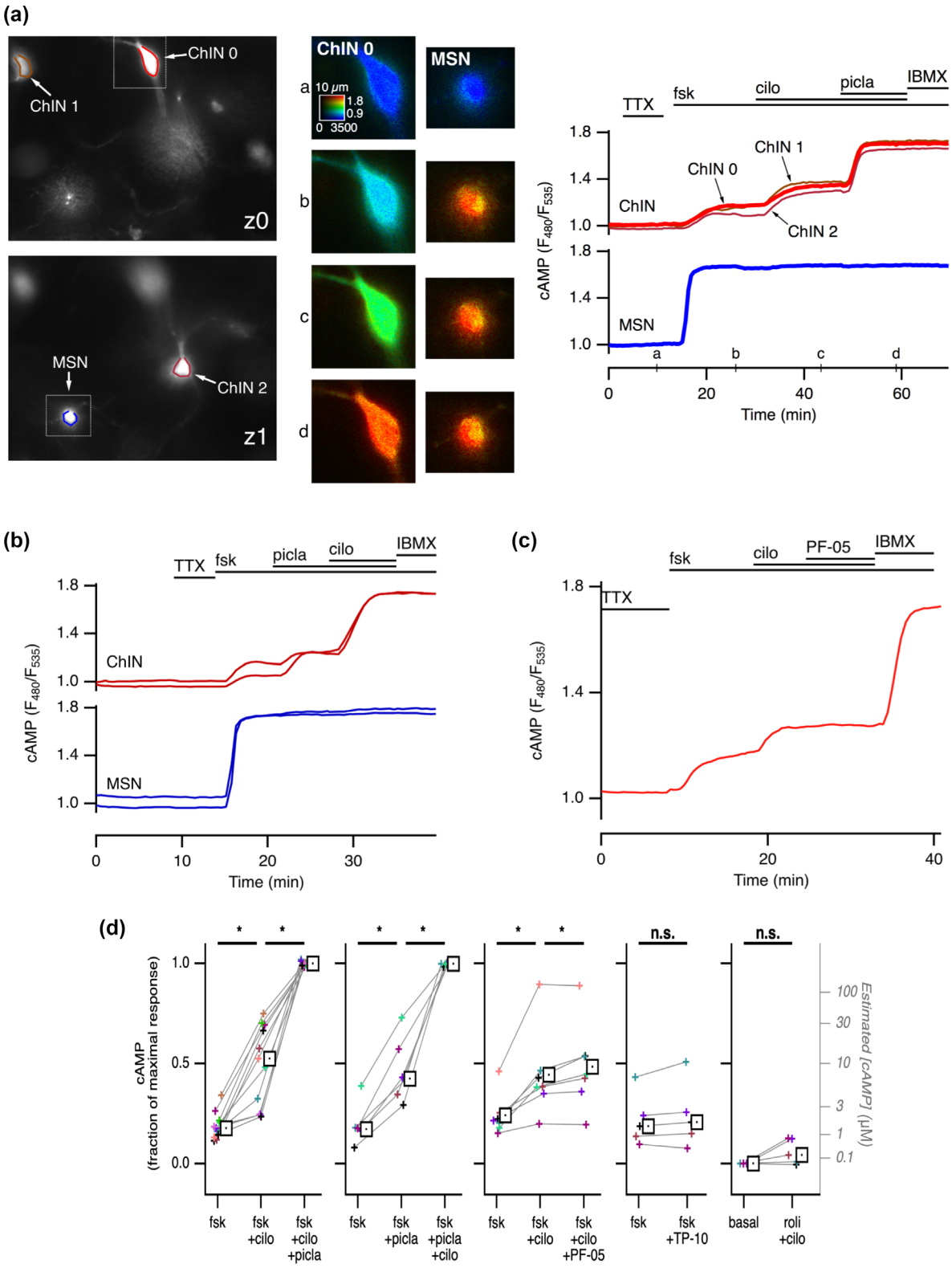

FIGURE 2 Legend on next page.

DEANO induced no further cAMP increase, indicating that cilostamide also occludes the effects of DEANO (Figure 3b, right panel). These experiments demonstrate that the activation of the cGMP pathway in striatal ChINs increases cAMP via PDE3 inhibition.

As a control, we confirmed, with the cGMP-selective biosensor cyGNAL (Betolngar et al., 2019), that bath application of DEANO (10 μM) induced a rapid and large increase in cGMP concentration in ChINs (Figure 3c). Preliminary experiments with 1 μM DEANO suggested less robust responses. Bath application of the inhibitor of soluble guanylyl cyclase **ODQ** (20 μM) had no effect (Figure 3d), showing a lack of basal cGMP production in our experimental conditions.

Altogether, these findings unequivocally establish that cGMP signalling increases cAMP levels in striatal ChINs by suppressing PDE3 activity. This signalling mechanism strikingly contrasts with cGMP effects in MSNs where it activates PDE2A and thus reduces cAMP level (Polito et al., 2013).

3.4 | The calcium pathway decreases cAMP and cGMP via PDE1 activation

We previously observed that, in MSNs, PDE1 activity efficiently regulates cAMP and cGMP signals in the presence of calcium (Betolngar et al., 2019), illustrating that PDE1 is an integrator of cyclic nucleotide and calcium signalling. This effect in MSNs is likely to be mediated by the PDE1B isoform (Lakics et al., 2010). The PDE1A isoform is expressed in ChINs (Polli & Kincaid, 1994), but its functional role has remained unexplored. Here, we tested whether PDE1A activity in ChINs might down-regulate cAMP and/or cGMP signals when activated by calcium. First, we established reliable protocols to increase intracellular calcium. We used the Twitch-2B ratiometric biosensor to measure the calcium signal triggered by **NMDA receptors** and **type I metabotropic glutamate receptors** (mGlu1/5) (Figure 4). NMDA receptors were activated transiently by **NMDA** released from the 'caged' precursor MNI-NMDA (100 μM) by a flash of UV light, as previously described (Betolngar et al., 2019). This protocol triggered a large and transient calcium increase in all ChINs tested, as well as in MSNs if present in the same field of view (Figure 4a). Figure 4b shows the calcium response to NMDA in ChINs with the average trace (left), and baseline and peak amplitude (right) for individual ChINs. We also observed that activation of mGlu1/5 receptors, by bath application of the selective agonist **DHPG** (50 μM), triggered a calcium increase of large amplitude and duration (Figure 4a, c). Interestingly, while mGlu1/5 receptors are also expressed in MSNs, no or little calcium response to DHPG was observed in these neurons.

We then tested whether such calcium increases activate PDE1 and therefore could reduce cAMP or cGMP. A steady-state elevated cAMP level was first obtained using forskolin and blocking PDE3 and PDE4 (with either 1 μM cilostamide and 1 μM **roflumilast** or 10 μM cilostamide and 1 μM piclamilast) and PDE2A (with PF-05, 1 μM). In order to stimulate a moderate cAMP production and thus maintain the visibility of PDE1 action, a lower concentration of forskolin (0.5 μM) was employed in these experiments. NMDA uncaging or DHPG bath application both produced large decreases in cAMP levels in ChIN (Figure 5a, c, e). These effects were largely reduced with **Lu AF64196** (1–10 μM), a potent and selective PDE1 inhibitor (Khammy et al., 2017) for NMDA and for DHPG. It should also be noted that, in the presence of the PDE1 inhibitor Lu AF64196, some changes in cAMP level still remained, which can result either from incomplete PDE1A inhibition and/or from NMDA effects on other targets such as calcium-modulated adenylyl cyclases.

We then tested whether the activation of PDE1 by calcium could also regulate cGMP level in ChINs. In these experiments, NMDA receptors were transiently activated by the MNI-NMDA uncaging protocol, and the mGlu1/5 receptors were activated with bath application of 1 μM **quisqualate** (AMPA and mGlu receptor agonist) in the presence of the AMPA receptor antagonist **NBQX** (1 μM) and NMDA antagonist **D-AP5** (20 μM). First, a steady-state cGMP level was obtained with a bath application of 10 μM DEANO. NMDA uncaging or activation of mGlu1/5 receptors both produced large decreases in cGMP levels in ChIN (Figure 6c, e). Again, these effects were largely reduced with Lu AF64196 (Figure 6d, f). As a control, we verified that PDE1 inhibition had no effect on the steady-state cGMP level elicited by 10 μM DEANO (Figure 7g).

Collectively, these experiments show that striatal ChINs express functional PDE1 that efficiently degrades both cAMP and cGMP in response to an increase in intracellular calcium.

FIGURE 2 **PDE3 and PDE4 are the main phosphodiesterases controlling cAMP in ChINs.** (a) The Epac-S^{H150} biosensor for cAMP was expressed in mouse pup striatal brain slices and imaged with wide-field microscopy. Two focal planes (z0 and z1) in the same field of view were acquired for each timepoint. Regions of interest shown on the greyscale images define the area used to measure the ratio (F480/F535) for three individual ChINs (red ROIs, ChIN 0 to 2, and red traces in the graph) and an MSN (blue ROI and blue trace in the graph). Dashed squares indicate the regions shown in pseudocolour for each timepoint (a-d) for a ChIN and an MSN. Horizontal bars on the graph indicate the bath application of drugs: tetrodotoxin (TTX, 0.2 μM), forskolin (fsk, 13 μM), cilostamide (cilo, 10 μM), piclamilast (picla, 1 μM) and IBMX (200 μM). (b) Same protocol as in Figure 2a except that the order of application of cilostamide and piclamilast was inverted. (c) Same protocol as in Figure 2a except that, instead of piclamilast, PF-05180999 (PF-05, 1 μM) was applied to inhibit PDE2A. (d) For each experiment, the average normalised ratio is measured over the steady-state ratio for each drug combination. If several ChINs were present in the same recording, their measurements are averaged. For each experiment, the successive measurements are plotted as markers with the same colour and connected by a line. The median of the repeated experiments is indicated with a square marker. * $P<0.05$, significantly different as indicated; n.s., not significant. Values were: fsk: 0.18; fsk + cilo: 0.52; fsk + cilo + picla: 1.00; $n = 11$; $N = 18$; $A = 7$; Friedman's rank test: $F = 22$; fsk: 0.17; fsk + picla: 0.42; fsk + picla + cilo: 1.00; $n = 6$; $N = 7$; $A = 4$; Friedman's rank test: $F = 12$; fsk: 0.22; fsk + cilo: 0.38; fsk + cilo + PF-05: 0.45; $n = 7$; $N = 13$; $A = 6$; Friedman's rank test: $F = 11.1$; fsk: 0.19; fsk + TP-10: 0.21; $n = 5$; $N = 7$; $A = 4$; roli + cilo: $n = 5$; $N = 6$; $A = 3$.

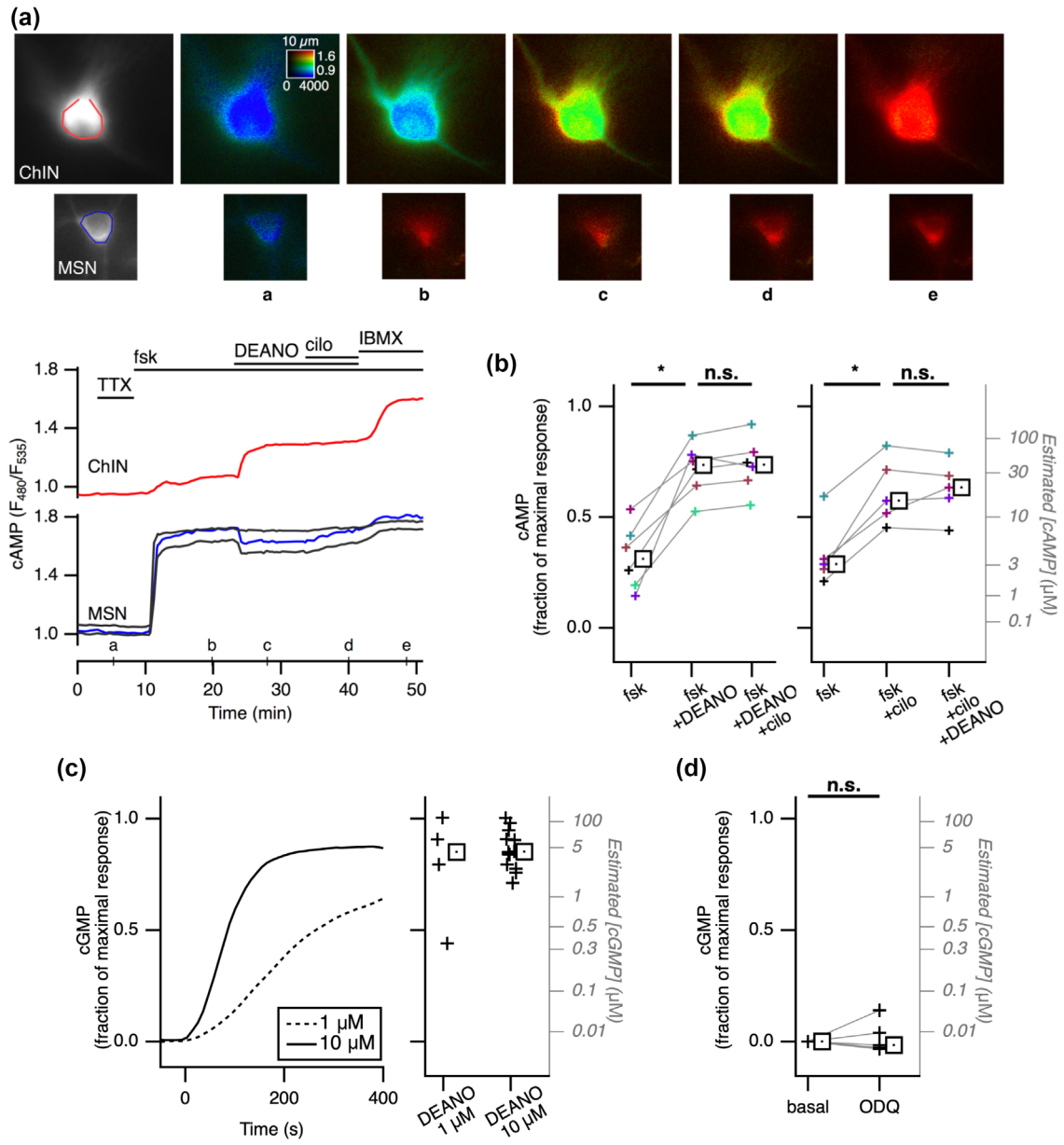

FIGURE 3 **NO donor increases intracellular cAMP through PDE3A inhibition.** (a) The Epac-S^{H150} biosensor for cAMP was expressed in striatal brain slices and imaged with wide-field microscopy. Images show a ChIN (top line) and an MSN (bottom line). Traces below show the ratio of these ROIs as well as other MSNs. (b, left) The same experiment was repeated 6 times. Plots display the average ratio: fsk: 0.31 of maximal response; fsk + DEANO: 0.73; fsk + DEANO + cilo: 0.74; $n = 6$, $N = 10$, $A = 5$; Friedman's rank test: $F = 10.3$. (b, right) Average ratio responses when cilo was applied before DEANO; fsk: 0.29; fsk + cilo: 0.57; fsk + cilo + DEANO: 0.63, n = 5, $N = 8$, $A = 4$; Friedman's rank test: $F = 7.6$. * $P<0.05$, significantly different as indicated; n.s., not significant. (c) The NO donor DEANO increases cGMP in ChINs. The cyGNAL biosensor for cGMP was used to monitor changes in intracellular cGMP concentration during the bath application of 1 or 10 µM DEANO. Traces on the left show that the average time course of the ratio increase for 1 or 10 µM DEANO in ChIN. The plot shows the steady-state ratio for each experiment as a cross marker. (d) The inhibitor of soluble guanylyl cyclase ODQ (20 µM) had no effect ($n = 5$; $N = 7$; $A = 1$). n.s., not significant.

4 | DISCUSSION

Our study highlights striking differences between striatal ChINs and MSNs in the way they handle cAMP signals. While MSNs rapidly reach a maximal response to forskolin, ChINs show slow and moderate increases in cAMP concentration. These observations reinforce the view that ChINs and MSNs express intrinsic differences in signal integration properties that endow them with fundamentally different functions in the striatal network. Among these differences, our experiments highlighted how the NO-cGMP pathway is differentially integrated in ChINs and in MSNs through the expression of different phosphodiesterases.

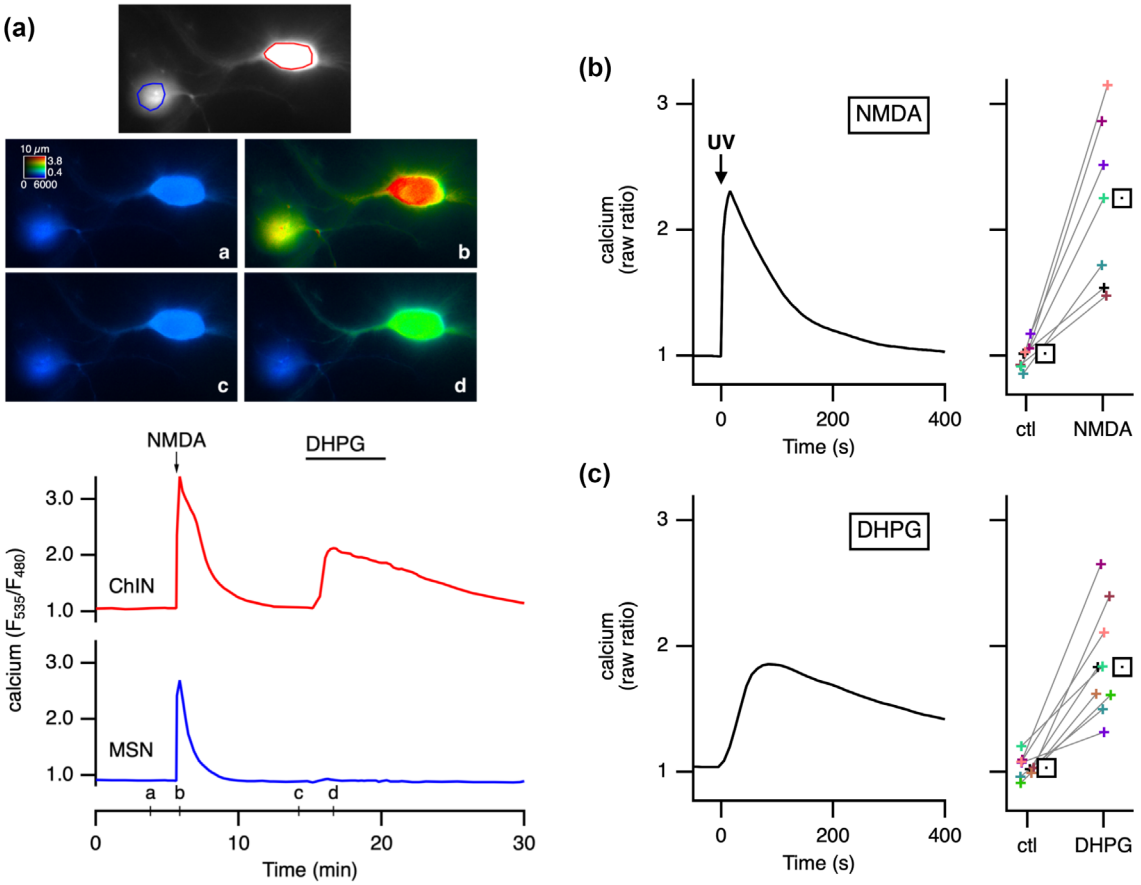

FIGURE 4 **NMDA photorelease or activation of group I mGlu receptors induces large calcium signals in ChIN.** The Twitch-2B calcium biosensor was expressed in striatal brain slices and imaged with wide-field microscopy. (a) Intracellular calcium is monitored over regions of interest drawn on a ChIN and on an MSN (red and blue, respectively). Release of NMDA from MNI-NMDA with a flash of UV light (arrow) raised calcium in both neurons, whereas sustained bath application of 50 μM DHPG, an agonist of group I metabotropic glutamate receptors, increased intracellular calcium levels selectively in ChIN. (b, c) The average time course of the ratio change triggered by NMDA and DHPG in ChIN is shown on the left; plots on the right display the baseline and peak ratio value measured in ChINs for independent experiments (b: $n = 7$, $N = 7$, $A = 4$; c: $n = 9$, $N = 9$, $A = 6$).

Previous transcriptomic and proteomic studies suggested the expression of specific phosphodiesterases in striatal ChIN (Polli & Kincaid, 1994; Reinhardt & Bondy, 1996; Saunders et al., 2018), but no functional analysis has been performed so far. We used highly specific phosphodiesterase inhibitors to acutely test the functional contribution of these phosphodiesterases. Our experiments demonstrate for the first time that PDE1, PDE3 and PDE4 are active in striatal ChINs and regulate the dynamics of cAMP in the context of neuromodulation by NO or glutamate (Figure 7). This specific combination of phosphodiesterases contrasts with the situation in MSNs which express PDE1B, PDE2A, PDE4 and PDE10A. In our experiments, we observed little or no signs of PDE2A or PDE10A activity in ChINs, consistent with the documented absence of their mRNA in these cells (Sano et al., 2008; Saunders et al., 2018; Xie et al., 2006). This finding contrasts with the important functional role played by PDE2A and PDE10A in MSNs (Mota et al., 2021; Polito et al., 2013, 2015). Overall, PDE3A emerges as a characteristic feature of striatal ChINs, along with the expression of PDE1A and PDE4.

Remarkably, because PDE3 is inhibited by cGMP, its presence in ChINs suggests potential cross-regulation of cAMP by the NO-cGMP signalling pathway, which was demonstrated by our experiments. Surprisingly, this interesting possibility had never been explored in neurons, while its demonstration in other physiological conditions remains scarce (Eckly & Lugnier, 1994; Komas et al., 1991; Maurice & Haslam, 1990). This mechanism has also been described in cardiomyocytes, with the added complexity of PDE2A being co-expressed with PDE3: depending on cAMP levels, NO donors either potentiate or reduce I_{Ca}, consistent with the inhibition of PDE3 or the activation of PDE2A. This effect has been reported in frog ventricular cardiomyocytes (Méry et al., 1993) as well as in human cardiomyocytes (Kirstein et al., 1995; Vandecasteele et al., 2001).

Our data show for the first time in neurons that the effect of the NO-cGMP neuromodulatory axis positively controls cAMP levels via PDE3 inhibition. This mechanism may be involved in the excitatory effect of NO donors documented in striatal ChINs, an effect mediated by the facilitation of I_h activation by cAMP (Blomeley et al., 2015; Centonze et al., 2001; Galati et al., 2008). While the NO/cGMP

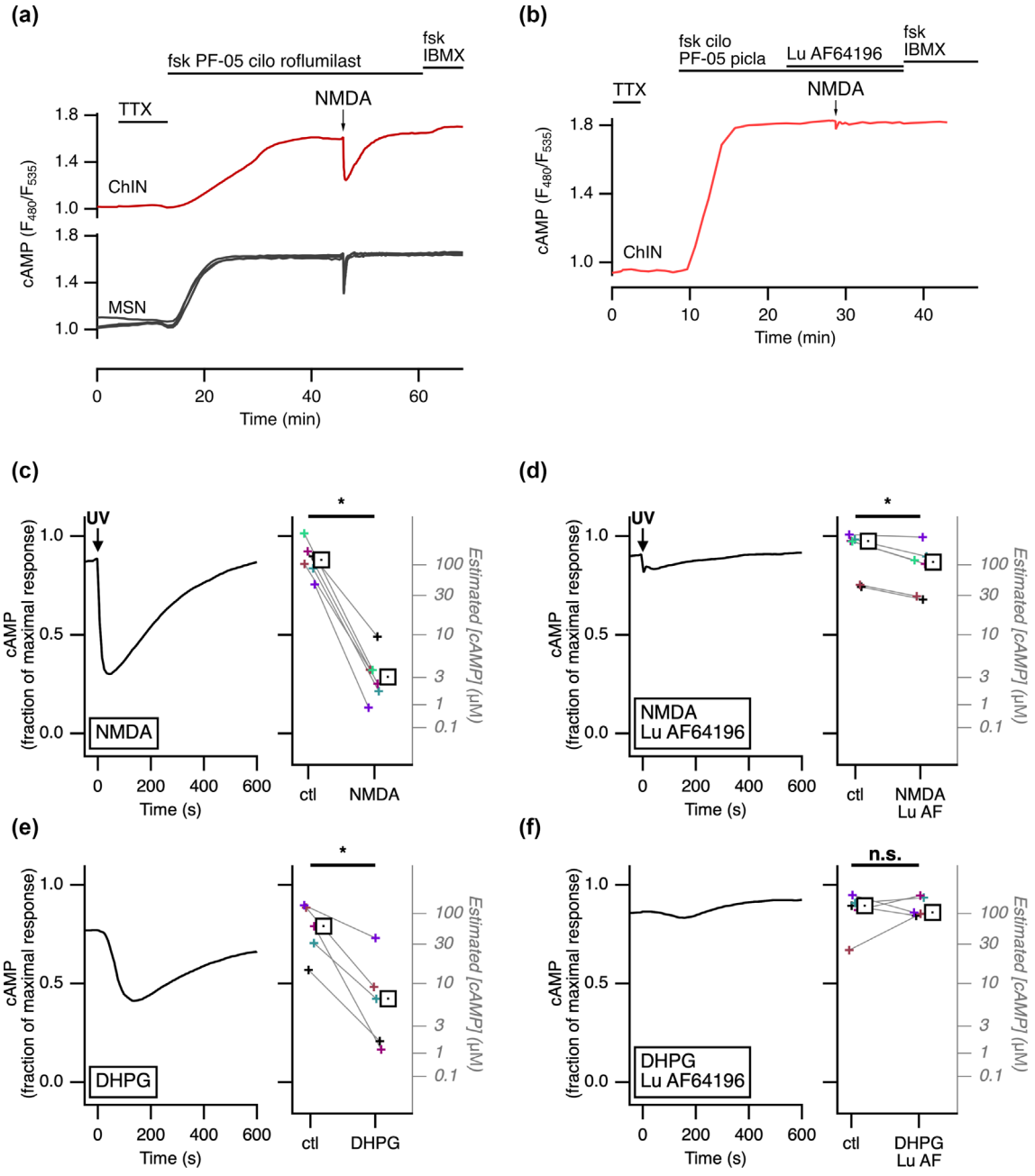

FIGURE 5 **Activation of NMDA or mGlu1/5 receptors in ChIN decreases cAMP via PDE1 activation.** The Epac-S^{H150} biosensor for cAMP was expressed in striatal brain slices, and ChINs were imaged with wide-field microscopy. (a) cAMP production was stimulated with 0.5 µM fsk in the presence of inhibitors of PDE2A (PF-05180999, 1 µM), PDE3 (cilo, 1 µM) and PDE4 (roflumilast, 1 µM). On the steady-state cAMP level, a flash of UV light at the time indicated by the arrow photoreleased NMDA from MNI-NMDA (100 µM), triggering a ratio decrease, in both ChIN and MSNs. (b) The selective PDE1 inhibitor Lu AF64196 (1 µM) prevented this decrease. (c–f) These experiments were repeated using phosphodiesterase inhibitors (PDE3: cilo, 1 µM or 10 µM; PDE4: roflumilast or piclamilast, 1 µM), (c) without or (d) with Lu AF64196 (1 or 10 µM). The graph shows the average normalised cAMP signal in ChINs, and the plot shows the amplitude of the steady-state cAMP level (ctl) and minimal cAMP level reached in response to NMDA photorelease (NMDA). A similar set of experiments was performed except that DHPG (50 µM) was applied in the bath. This also induced a transient decrease in (e) cAMP concentration. This decrease was suppressed by (f) Lu AF64196. In control conditions (Figure 5c and e), values were before NMDA photorelease: 0.88 of Rmax, NMDA application: 0.29, $n = 6$, $N = 9$, $A = 5$; before DHPG: 0.79, DHPG application: 0.42, $n = 5$, $N = 7$, $A = 4$. In the presence of Lu AF64196, values were: before NMDA photorelease: 0.97 of Rmax, after: 0.87, $n = 6$, $N = 9$, $A = 4$; before DHPG: 0.89, DHPG application: 0.86, $n = 5$, $N = 8$, $A = 3$. The ratio change was reduced by Lu AF64196. * $P<0.05$, significantly different as indicated; n.s., not significant.

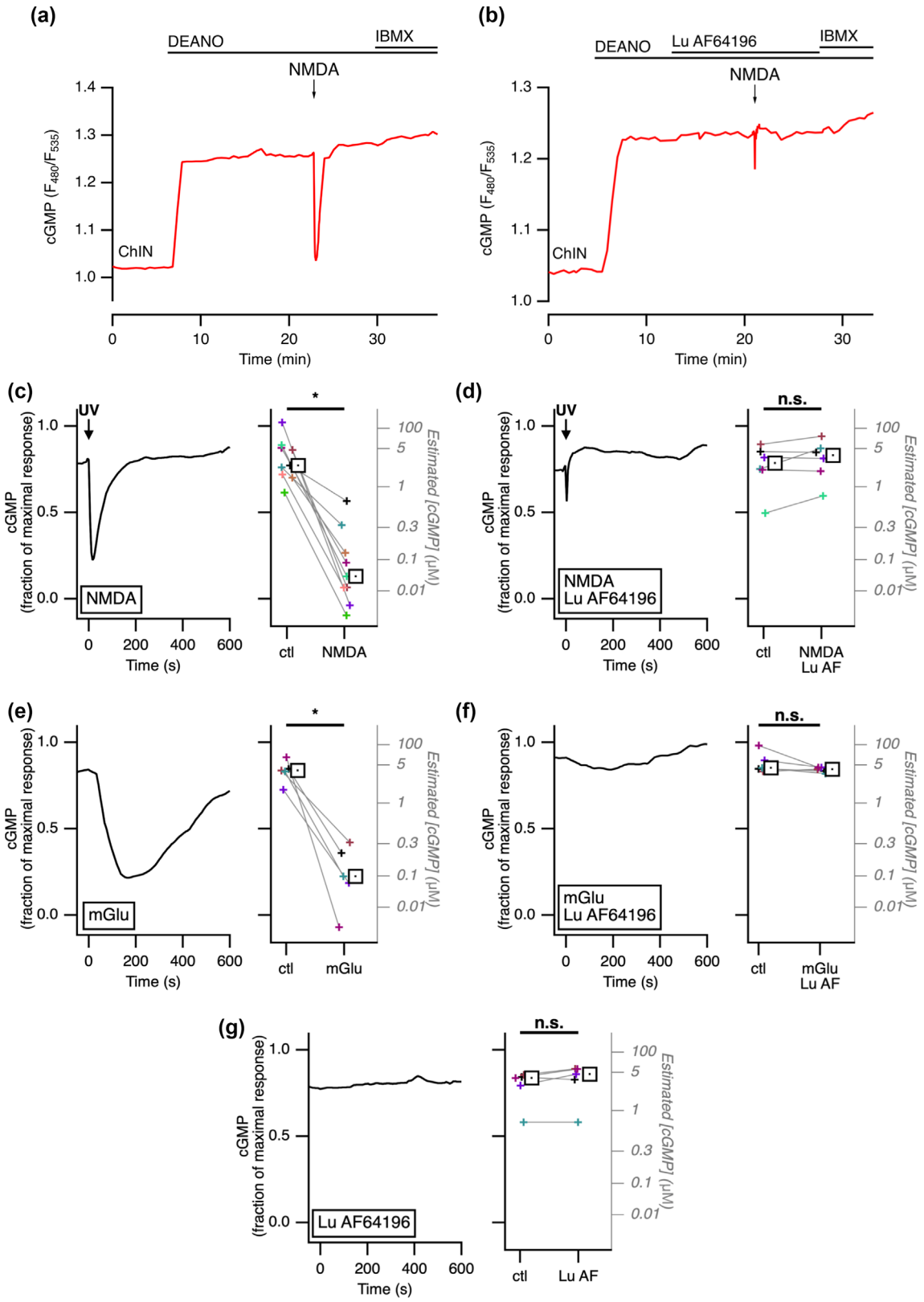

FIGURE 6 Legend on next page.

pathway has long been known to play an important role in striatal function by regulating excitability, dopamine release and synaptic transmission (Blomeley et al., 2015; Calabresi et al., 1999; Hartung et al., 2011; Padovan-Neto & West, 2017; West et al., 2002; West & Grace, 2000; West & Tseng, 2011), our work suggests a novel mechanism whereby NO-induced PDE3 inhibition would mediate an increase in acetylcholine release by striatal ChINs. Importantly, this NO-mediated increase in cAMP levels observed in ChINs sharply contrasts with its effect in MSNs, where, by stimulating PDE2A, NO donors down-regulate cAMP signalling (Lin et al., 2010; Polito et al., 2013).

Pharmacological inhibition of PDE3 is used in the treatment of some clinical conditions of the cardiovascular system. PDE3 inhibitors such as **milrinone** exert powerful positive inotropic and lusitropic effects and are used in the treatment of acute heart failure (Movsesian et al., 2011). Milrinone also prevented the delayed ischemic injury in the brain (Bernier et al., 2021; Castle-Kirszbaum et al., 2021; Fraticelli et al., 2008). However, while several preclinical and clinical studies showed beneficial effects of PDE3 inhibitors in neuronal functions, whether these effects result from a direct action on neurons or indirect effects through the improvement of the vascular condition remains uncertain and should be evaluated specifically. Our observations may be of particular significance in the context of pathological conditions such as Parkinson's disease. Indeed, the first medications for Parkinson's disease were anticholinergic drugs, and there is compelling evidence that photo-inhibition of striatal ChINs has prominent anti-parkinsonian effects (Maurice et al., 2015; Ztaou et al., 2016). A noteworthy observation is that the NO-mediated increase in ChIN firing is markedly more pronounced in a mouse model of Parkinson's disease (Galati et al., 2008). This suggests that pharmacological moderation of striatal ChIN activity might reduce some symptoms of Parkinson's disease. In the course of this disease, chronic treatment with **L-DOPA** eventually leads to dyskinesia. Surprisingly, both potentiation and inhibition of the NO/cGMP pathway reduce these abnormal involuntary movements (see Padovan-Neto & West, 2017). Such paradoxical effects can result from complex interplays between MSNs of direct and indirect pathways where the NO/cGMP simultaneously affects cAMP through PDE2A stimulation (Lin et al., 2010; Polito et al., 2013) and DARPP-32 phosphorylation via PKG (Calabresi et al., 2000). Our data highlight the striatal ChINs as novel actors in this game, and the NO/cGMP/PDE3 pathway should be taken into account when considering the physiology of the striatum.

Another cross-pathway integration level is provided by PDE1, which powerfully degrades both cAMP and cGMP when activated by calcium-calmodulin (Goraya & Cooper, 2005). Calcium imaging experiments showed that while activating NMDA receptors increased intracellular calcium, the ChINs also displayed a powerful and sustained calcium signal in response to the activation of group I metabotropic glutamate receptors. This is consistent with the expression of mGlu1 and mGlu5 receptors (Bell et al., 2002; Kerner et al., 1997; Mitrano & Smith, 2007; Tallaksen-Greene et al., 1998), which are known to couple through G_q/G_{11} to the release of intracellular calcium stores. In this study, the stimulation of both NMDA and group I metabotropic receptors efficiently reduced intracellular cAMP and cGMP, an effect similar to that reported previously in MSNs (Betolngar et al., 2019). We hypothesise that this effect is mediated by PDE1A in ChINs, whereas PDE1B is expressed in MSNs (Polli & Kincaid, 1994; Saunders et al., 2018).

In the last decade, the pharmacological inhibition of PDE1 has attracted considerable interest, particularly in the context of CNS diseases (Wennogle et al., 2017). Among the various PDE1 inhibitors under investigation, Lu AF64386 has shown promising results in reduction of impulsivity and reversal of neurophysiological deficits in the rat phencyclidine model of schizophrenia (Hayes et al., 2021), indicating that PDE1 inhibition may be beneficial in disorders involving a dysfunction of the medial prefrontal cortex and nucleus accumbens network. Another line of research has highlighted PDE1 inhibitors as pro-cognitive and memory enhancing (Dyck et al., 2017; Enomoto et al., 2019). PDE1 inhibitors have also demonstrated anti-parkinsonian effects, particularly potentiating the effects of **levodopa** in rodent and monkey models of Parkinson's disease, as well as having potent efficacy against levodopa-induced dyskinesia (Enomoto et al., 2021). In a Phase 1b research on Parkinson's disease in humans, a PDE1 inhibitor has shown therapeutic effects, and currently, **lenrispodun** is in Phase 2 clinical trial (NCT05766813). Our data support the notion that PDE1 plays a role in the integration of calcium and cyclic nucleotide signalling in striatal ChINs. In other types of

FIGURE 6 **Activation of NMDA or mGlu1/5 receptors in ChIN decreases cGMP via PDE1 activation.** The cyGNAL biosensor for cGMP was expressed in striatal brain slices, and ChINs were imaged with wide-field microscopy. (a) cGMP production was stimulated with 10 μM DEANO. On the steady-state cGMP level, a flash of UV light at the time indicated by the arrow photoreleased NMDA from MNI-NMDA (100 μM), triggering a ratio decrease. (b) The selective PDE1 inhibitor Lu AF64196 (10 μM) prevented this decrease. These experiments were repeated (c) without or (d) with Lu AF64196 (1 or 10 μM). The graph shows the average normalised cGMP signal, and the plot shows the amplitude of the steady-state cGMP level (ctl) and minimal cGMP level reached in response to NMDA photorelease (NMDA). A similar set of experiments was performed except that mGlu1/5 receptors were activated by bath application of quisqualate (1 μM) together with AMPA receptor antagonist NBQX (1 μM) and NMDA antagonist D-AP5 (20 μM). This also induced a transient decrease in (e) cGMP concentration. This decrease was also suppressed by (f) Lu AF64196. (c, e) In control condition, values were: before NMDA photorelease: 0.77 of Rmax, after: 0.13, $n = 9$, $N = 13$, $A = 9$; before quisqualate: 0.84, quisqualate application: 0.22, $n = 5$, $N = 9$, $A = 4$. In the presence of (d, f) Lu AF64196: before NMDA photorelease: 0.78 of Rmax, after: 0.83, $n = 6$, $N = 7$, $A = 6$; before quisqualate: 0.85, quisqualate application: 0.84, $n = 5$, $N = 7$, $A = 3$. The ratio change was significantly reduced by Lu AF64196. (g) Lack of effect of Lu AF64196: in DEANO: 0.83 of Rmax; in DEANO and Lu AF64196: 0.85; $n = 5$, $N = 6$, $A = 5$. * $P<0.05$, significantly different as indicated; n.s., not significant.

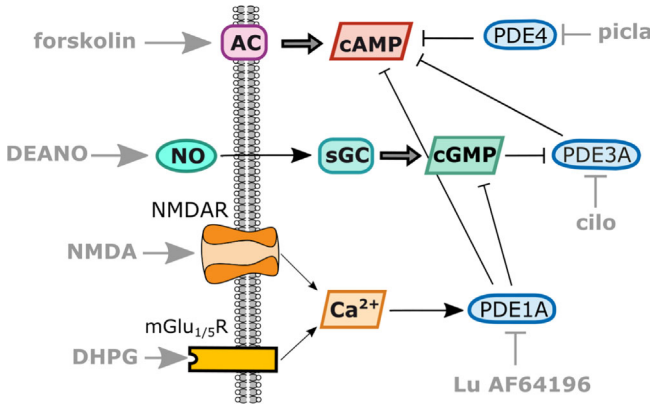

FIGURE 7 Schematic representation of phosphodiesterases and cross-pathway regulations in striatal ChINs.

neurons, PDE1 has been shown to control the calcium threshold for synaptic plasticity (Kitagawa et al., 2009), but the precise physiological function of cyclic nucleotide and calcium signalling in ChINs is still unknown. Further investigations combining multifaceted techniques and behavioural assays are needed to understand the influence of PDE1A and PDE1B isoforms on neuronal networks and behaviour.

The co-expression of PDE1A and PDE3A in striatal ChINs raises the intriguing question of what happens in physiological situations when glutamatergic inputs occur simultaneously with NO release: activation of PDE1A by calcium is expected to reduce cAMP levels, while PDE3A inhibition by cGMP should increase cAMP. PDE3A has a sub-micromolar Km for cAMP (Sudo et al., 2000) whereas PDE1 has a much higher Km value (Poppe et al., 2008), suggesting that, on low cAMP levels, cGMP-mediated inhibition of PDE3A should win against PDE1A and therefore raise cAMP level. However, PDE1A also degrades cGMP, which implies that it may temper the effects of NO on the cAMP pathway. Predicting the precise interplay of these effects within ChINs thus appears challenging. Furthermore, the possibility of phosphodiesterases residing in distinct sub-cellular signalling domains can substantially alter their overall impact. Ultimately, the integrated response will be shaped by the kinetics governing these events relative to one another.

The low responsiveness of striatal ChINs to cAMP-activating signals such as forskolin is striking but the underlying cellular mechanisms remain to be determined. All adenylyl cyclases except AC9 are activated by forskolin (Defer et al., 2000). **AC1**, **AC2** and **AC5** are widely expressed in the brain, including the striatum (Matsuoka et al., 1997). Cluster analysis of mRNA transcript suggest that AC1 and AC2 predominate in striatal ChINs whereas AC5 would dominate in MSNs (Saunders et al., 2018). This indicates that the reduced responsiveness to forskolin in ChINs, compared to MSNs, does not result from ChINs lacking adenylyl cyclases sensitive to forskolin. Another important factor is the amount of active signalling enzyme, that is, the density of cyclase per membrane surface or amount of calcium-store per cytosolic volume, in relation with cell geometry. Indeed, striatal ChINs have a large soma, their proximal dendrites have a large diameter compared to the much thinner MSNs (Tepper et al., 2010, 2018). Surface to volume ratio critically determines whether a signal gets amplified or dampened (Neves et al., 2008) and, in the case of cAMP, small neurons like MSNs can accumulate cAMP more easily. In contrast, ChINs with a larger cytosol in which cAMP gets degraded by phosphodiesterases are in a less favourable position to accumulate enough cAMP to be detected by our cytosolic biosensors.

The way in which these cellular events come together within the network remains poorly understood. However, our data strongly suggest that this new cGMP-mediated up-regulation of cAMP signalling should be considered in physiological scenarios. **Somatostatin**- and **NPY**-positive interneurons express **NO synthase** and are the primary NO source in the striatum (Tepper et al., 2010, 2018). The release of NO depends on intracellular calcium levels and is heightened by dopamine (Centonze et al., 2002; West & Tseng, 2011). The convergence of glutamatergic and dopaminergic inputs is thus expected to trigger the release of NO, which should favour ChINs excitability via the cGMP/PDE3A/cAMP mechanism. Future studies should concentrate on whether this mechanism contributes to the rebound excitation observed in striatal ChINs following phasic dopamine release or contributes to the broader regulation of striatal ChIN activity.

AUTHOR CONTRIBUTIONS

Bompierre, S.: Conceptualisation (equal); data curation (equal); investigation (lead); validation (equal); writing—original draft (equal), writing—review and editing (equal). **Byelyayeva, Y.:** Conceptualisation (equal); investigation (equal); writing—review and editing (supporting). **Mota, E.:** Conceptualisation (equal); investigation (equal); writing—review and editing (supporting). **Lefevre, M.:** Conceptualisation (equal); investigation (equal); writing—review and editing (supporting). **Pumo, A.:** Conceptualisation (equal); investigation (equal); writing—review and editing (supporting). **Kehler, J.:** Conceptualisation (supporting); resources (equal); writing—review and editing (supporting). **Castro, L. R. V.:** Conceptualisation (equal); data curation (equal); funding acquisition (equal); investigation (supporting); methodology (equal); project administration (equal); supervision (supporting); validation (equal); writing—original draft (equal); writing—review and editing (equal). **Vincent, P.:** *(Corresponding Author)*, conceptualisation (equal); data curation (lead); formal analysis (lead); funding acquisition (equal); investigation (supporting); methodology (equal); project administration (equal); software (lead); supervision (lead); validation (equal); visualisation (equal); writing—original draft (equal); writing—review and editing (equal).

ACKNOWLEDGEMENTS

We would like to gratefully thank Drs Corinne Beurrier, Julie Perroy and Pr Juan Llopis for their careful reading and helpful comments on this manuscript. This work was supported by Association France Parkinson and by the Investissements d'Avenir programme managed by the ANR under reference ANR-11-IDEX-0004-02.

CONFLICT OF INTEREST STATEMENT

The authors have no conflicts of interest to declare.

DATA AVAILABILITY STATEMENT

Data are available from the corresponding author upon reasonable request.

DECLARATION OF TRANSPARENCY AND SCIENTIFIC RIGOUR

This declaration acknowledges that this paper adheres to the principles for transparent reporting and scientific rigour of preclinical research as stated in the BJP guidelines for Design and Analysis, and Immunoblotting and Immunochemistry, and as recommended by funding agencies, publishers and other organisations engaged with supporting research.

ORCID

Ségolène Bompierre https://orcid.org/0000-0003-1140-4409
Elia Mota https://orcid.org/0000-0003-4393-5781
Liliana R. V. Castro https://orcid.org/0000-0001-8902-089X
Pierre Vincent https://orcid.org/0000-0002-8479-1908

REFERENCES

Alexander, S. P. H., Christopoulos, A., Davenport, A. P., Kelly, E., Mathie, A. A., Peters, J. A., Veale, E. L., Armstrong, J. F., Faccenda, E., Harding, S. D., Davies, J. A., Abbracchio, M. P., Abraham, G., Agoulnik, A., Alexander, W., Al-Hosaini, K., Bäck, M., Baker, J. G., Barnes, N. M., … Ye, R. D. (2023). The Concise Guide to PHARMACOLOGY 2023/24: G protein-coupled receptors. *British Journal of Pharmacology*, *180*(Suppl 2), S23–S144. https://doi.org/10.1111/bph.16177

Alexander, S. P. H., Fabbro, D., Kelly, E., Mathie, A. A., Peters, J. A., Veale, E. L., Armstrong, J. F., Faccenda, E., Harding, S. D., Davies, J. A., Annett, S., Boison, D., Burns, K. E., Dessauer, C., Gertsch, J., Helsby, N. A., Izzo, A. A., Ostrom, R., Papapetropoulos, A., … Wong, S. S. (2023). The Concise Guide to PHARMACOLOGY 2023/24: Enzymes. *British Journal of Pharmacology*, *180*(Suppl 2), S289–S373. https://doi.org/10.1111/bph.16181

Alexander, S. P. H., Mathie, A. A., Peters, J. A., Veale, E. L., Striessnig, J., Kelly, E., Armstrong, J. F., Faccenda, E., Harding, S. D., Davies, J. A., Aldrich, R. W., Attali, B., Baggetta, A. M., Becirovic, E., Biel, M., Bill, R. M., Caceres, A. I., Catterall, W. A., Conner, A. C., … Zhu, M. (2023). The Concise Guide to PHARMACOLOGY 2023/24: Ion channels. *British Journal of Pharmacology*, *180*(Suppl 2), S145–S222. https://doi.org/10.1111/bph.16181

Aosaki, T., Kiuchi, K., & Kawaguchi, Y. (1998). Dopamine D1-like receptor activation excites rat striatal large aspiny neurons in vitro. *The Journal of Neuroscience*, *18*(14), 5180–5190. https://doi.org/10.1523/JNEUROSCI.18-14-05180.1998

Aosaki, T., Miura, M., Suzuki, T., Nishimura, K., & Masuda, M. (2010). Acetylcholine-dopamine balance hypothesis in the striatum: An update. *Geriatrics & Gerontology International*, *10*(Suppl 1), S148–S157. https://doi.org/10.1111/j.1447-0594.2010.00588.x

Bell, M. I., Richardson, P. J., & Lee, K. (2002). Functional and molecular characterization of metabotropic glutamate receptors expressed in rat striatal cholinergic interneurones. *Journal of Neurochemistry*, *81*(1), 142–149. https://doi.org/10.1046/j.1471-4159.2002.00815.x

Bender, A. T., & Beavo, J. A. (2006). Cyclic nucleotide phosphodiesterases: Molecular regulation to clinical use. *Pharmacological Reviews*, *58*(3), 488–520. https://doi.org/10.1124/pr.58.3.5

Bennett, B. D., Callaway, J. C., & Wilson, C. J. (2000). Intrinsic membrane properties underlying spontaneous tonic firing in neostriatal cholinergic interneurons. *The Journal of Neuroscience*, *20*(22), 8493–8503. https://doi.org/10.1523/JNEUROSCI.20-22-08493.2000

Bernier, T. D., Schontz, M. J., Izzy, S., Chung, D. Y., Nelson, S. E., Leslie-Mazwi, T. M., Henderson, G. V., Dasenbrock, H., Patel, N., Aziz-Sultan, M. A., Feske, S., du, R., Abulhasan, Y. B., & Angle, M. R. (2021). Treatment of subarachnoid hemorrhage-associated delayed cerebral ischemia with milrinone: A review and proposal. *Journal of Neurosurgical Anesthesiology*, *33*(3), 195–202. https://doi.org/10.1097/ANA.0000000000000755

Betolngar, D. B., Mota, É., Fabritius, A., Nielsen, J., Hougaard, C., Christoffersen, C. T., Yang, J., Kehler, J., Griesbeck, O., Castro, L. R. V., & Vincent, P. (2019). Phosphodiesterase 1 bridges glutamate inputs with NO- and dopamine-induced cyclic nucleotide signals in the striatum. *Cerebral Cortex*, *29*(12), 5022–5036. https://doi.org/10.1093/cercor/bhz041

Blomeley, C. P., Cains, S., & Bracci, E. (2015). Dual nitrergic/cholinergic control of short-term plasticity of corticostriatal inputs to striatal projection neurons. *Frontiers in Cellular Neuroscience*, *9*, 453. https://doi.org/10.3389/fncel.2015.00453

Börner, S., Schwede, F., Schlipp, A., Berisha, F., Calebiro, D., Lohse, M. J., & Nikolaev, V. O. (2011). FRET measurements of intracellular cAMP concentrations and cAMP analog permeability in intact cells. *Nature Protocols*, *6*(4), 427–438. https://doi.org/10.1038/nprot.2010.198

Butt, E., Nolte, C., Schulz, S., Beltman, J., Beavo, J. A., Jastorff, B., & Walter, U. (1992). Analysis of the functional role of cGMP-dependent protein kinase in intact human platelets using a specific activator 8-para-chlorophenylthio-cGMP. *Biochemical Pharmacology*, *43*(12), 2591–2600. https://doi.org/10.1016/0006-2952(92)90148-C

Calabresi, P., Gubellini, P., Centonze, D., Picconi, B., Bernardi, G., Chergui, K., Svenningsson, P., Fienberg, A. A., & Greengard, P. (2000). Dopamine and cAMP-regulated phosphoprotein 32 kDa controls both striatal long-term depression and long-term potentiation, opposing forms of synaptic plasticity. *The Journal of Neuroscience*, *20*(22), 8443–8451. https://doi.org/10.1523/JNEUROSCI.20-22-08443.2000

Calabresi, P., Gubellini, P., Centonze, D., Sancesario, G., Morello, M., Giorgi, M., Pisani, A., & Bernardi, G. (1999). A critical role of the nitric oxide/cGMP pathway in corticostriatal long-term depression. *The Journal of Neuroscience*, *19*(7), 2489–2499. https://doi.org/10.1523/JNEUROSCI.19-07-02489.1999

Castle-Kirszbaum, M., Lai, L., Maingard, J., Asadi, H., Danks, R. A., Goldschlager, T., & Chandra, R. V. (2021). Intravenous milrinone for treatment of delayed cerebral ischaemia following subarachnoid haemorrhage: A pooled systematic review. *Neurosurgical Review*, *44*(6), 3107–3124. https://doi.org/10.1007/s10143-021-01509-1

Centonze, D., Bracci, E., Pisani, A., Gubellini, P., Bernardi, G., & Calabresi, P. (2002). Activation of dopamine D1-like receptors excites LTS interneurons of the striatum. *The European Journal of Neuroscience*, *15*(12), 2049–2052. https://doi.org/10.1046/j.1460-9568.2002.02052.x

Centonze, D., Pisani, A., Bonsi, P., Giacomini, P., Bernardi, G., & Calabresi, P. (2001). Stimulation of nitric oxide-cGMP pathway excites striatal cholinergic interneurons via protein kinase G activation. *The Journal of Neuroscience*, *21*(4), 1393–1400. https://doi.org/10.1523/JNEUROSCI.21-04-01393.2001

Chen, Y., Granger, A. J., Tran, T., Saulnier, J. L., Kirkwood, A., & Sabatini, B. L. (2017). Endogenous Gαq-coupled neuromodulator receptors activate protein kinase A. *Neuron*, *96*, 1070–1083.e5. https://doi.org/10.1016/j.neuron.2017.10.023

Chen, Y., Saulnier, J. L., Yellen, G., & Sabatini, B. L. (2014). A PKA activity sensor for quantitative analysis of endogenous GPCR signaling via 2-photon FRET-FLIM imaging. *Frontiers in Pharmacology*, *5*, 56. https://doi.org/10.3389/fphar.2014.00056

Curtis, M. J., Alexander, S. P., Cirino, G., George, C. H., Kendall, D. A., Insel, P. A., Izzo, A. A., Ji, Y., Panettieri, R. A., Patel, H. H., Sobey, C. G., Stanford, S. C., Stanley, P., Stefanska, B., Stephens, G. J.,

Teixeira, M. M., Vergnolle, N., & Ahluwalia, A. (2022). Planning experiments: Updated guidance on experimental design and analysis and their reporting III. *British Journal of Pharmacology*, *179*, 3907–3913. https://doi.org/10.1111/bph.15868

Defer, N., Best-Belpomme, M., & Hanoune, J. (2000). Tissue specificity and physiological relevance of various isoforms of adenylyl cyclase. *American Journal of Physiology. Renal Physiology*, *279*(3), F400–F416. https://doi.org/10.1152/ajprenal.2000.279.3.F400

Deng, P., Zhang, Y., & Xu, Z. C. (2007). Involvement of I(h) in dopamine modulation of tonic firing in striatal cholinergic interneurons. *The Journal of Neuroscience*, *27*(12), 3148–3156. https://doi.org/10.1523/JNEUROSCI.5535-06.2007

Dyck, B., Branstetter, B., Gharbaoui, T., Hudson, A. R., Breitenbucher, J. G., Gomez, L., Botrous, I., Marrone, T., Barido, R., Allerston, C. K., Cedervall, E. P., Xu, R., Sridhar, V., Barker, R., Aertgeerts, K., Schmelzer, K., Neul, D., Lee, D., Massari, M. E., … Tabatabaei, A. (2017). Discovery of selective phosphodiesterase 1 inhibitors with memory enhancing properties. *Journal of Medicinal Chemistry*, *60*(8), 3472–3483. https://doi.org/10.1021/acs.jmedchem.7b00302

Eckly, A. E., & Lugnier, C. (1994). Role of phosphodiesterases III and IV in the modulation of vascular cyclic AMP content by the NO/cyclic GMP pathway. *British Journal of Pharmacology*, *113*(2), 445–450. https://doi.org/10.1111/j.1476-5381.1994.tb17009.x

Ehrengruber, M. U., Lundstrom, K., Schweitzer, C., Heuss, C., Schlesinger, S., & Gähwiler, B. H. (1999). Recombinant Semliki Forest virus and Sindbis virus efficiently infect neurons in hippocampal slice cultures. *Proceedings of the National Academy of Sciences of the United States of America*, *96*(12), 7041–7046. https://doi.org/10.1073/pnas.96.12.7041

Enomoto, T., Nakako, T., Goda, M., Wada, E., Kitamura, A., Fujii, Y., & Ikeda, K. (2021). A novel phosphodiesterase 1 inhibitor reverses L-dopa-induced dyskinesia, but not motivation deficits, in monkeys. *Pharmacology, Biochemistry, and Behavior*, *205*, 173183. https://doi.org/10.1016/j.pbb.2021.173183

Enomoto, T., Tatara, A., Goda, M., Nishizato, Y., Nishigori, K., Kitamura, A., Kamada, M., Taga, S., Hashimoto, T., Ikeda, K., & Fujii, Y. (2019). A novel phosphodiesterase 1 inhibitor DSR-141562 exhibits efficacies in animal models for positive, negative, and cognitive symptoms associated with schizophrenia. *The Journal of Pharmacology and Experimental Therapeutics*, *371*(3), 692–702. https://doi.org/10.1124/jpet.119.260869

Fraticelli, A. T., Cholley, B. P., Losser, M. R., Saint Maurice, J. P., & Payen, D. (2008). Milrinone for the treatment of cerebral vasospasm after aneurysmal subarachnoid hemorrhage. *Stroke*, *39*(3), 893–898. https://doi.org/10.1161/STROKEAHA.107.492447

Galati, S., D'angelo, V., Scarnati, E., Stanzione, P., Martorana, A., Procopio, T., Sancesario, G., & Stefani, A. (2008). In vivo electrophysiology of dopamine-denervated striatum: Focus on the nitric oxide/cGMP signaling pathway. *Synapse*, *62*(6), 409–420. https://doi.org/10.1002/syn.20510

Goraya, T. A., & Cooper, D. M. (2005). Ca2+−calmodulin-dependent phosphodiesterase (PDE1): Current perspectives. *Cellular Signalling*, *17*(7), 789–797. https://doi.org/10.1016/j.cellsig.2004.12.017

Gritton, H. J., Howe, W. M., Romano, M. F., DiFeliceantonio, A. G., Kramer, M. A., Saligrama, V., Bucklin, M. E., Zemel, D., & Han, X. (2019). Unique contributions of parvalbumin and cholinergic interneurons in organizing striatal networks during movement. *Nature Neuroscience*, *22*(4), 586–597. https://doi.org/10.1038/s41593-019-0341-3

Grynkiewicz, G., Poenie, M., & Tsien, R. Y. (1985). A new generation of Ca2+ indicators with greatly improved fluorescence properties. *The Journal of Biological Chemistry*, *260*(6), 3440–3450. https://doi.org/10.1016/S0021-9258(19)83641-4

Hartung, H., Threlfell, S., & Cragg, S. J. (2011). Nitric oxide donors enhance the frequency dependence of dopamine release in nucleus accumbens. *Neuropsychopharmacology*, *36*(9), 1811–1822. https://doi.org/10.1038/npp.2011.62

Hayes, J., Laursen, B., Eneberg, E., Kehler, J., Rasmussen, L. K., Langgard, M., Bastlund, J. F., & Gerdjikov, T. V. (2021). Phosphodiesterase type 1 inhibition alters medial prefrontal cortical activity during goal-driven behaviour and partially reverses neurophysiological deficits in the rat phencyclidine model of schizophrenia. *Neuropharmacology*, *186*, 108454. https://doi.org/10.1016/j.neuropharm.2021.108454

Herget, S., Lohse, M. J., & Nikolaev, V. O. (2008). Real-time monitoring of phosphodiesterase inhibition in intact cells. *Cellular Signalling*, *20*(8), 1423–1431. https://doi.org/10.1016/j.cellsig.2008.03.011

Howe, M., Ridouh, I., Allegra Mascaro, A. L., Larios, A., Azcorra, M., & Dombeck, D. A. (2019). Coordination of rapid cholinergic and dopaminergic signaling in striatum during spontaneous movement. *eLife*, *8*, e44903. https://doi.org/10.7554/eLife.44903

Kawaguchi, Y. (1992). Large aspiny cells in the matrix of the rat neostriatum in vitro: Physiological identification, relation to the compartments and excitatory postsynaptic currents. *Journal of Neurophysiology*, *67*(6), 1669–1682. https://doi.org/10.1152/jn.1992.67.6.1669

Kawaguchi, Y. (1993). Physiological, morphological, and histochemical characterization of three classes of interneurons in rat neostriatum. *The Journal of Neuroscience*, *13*(11), 4908–4923. https://doi.org/10.1523/JNEUROSCI.13-11-04908.1993

Keravis, T., & Lugnier, C. (2012). Cyclic nucleotide phosphodiesterase (PDE) isozymes as targets of the intracellular signalling network: Benefits of PDE inhibitors in various diseases and perspectives for future therapeutic developments. *British Journal of Pharmacology*, *165*(5), 1288–1305. https://doi.org/10.1111/j.1476-5381.2011.01729.x

Kerner, J. A., Standaert, D. G., Penney, J. B., Young, A. B., & Landwehrmeyer, G. B. (1997). Expression of group one metabotropic glutamate receptor subunit mRNAs in neurochemically identified neurons in the rat neostriatum, neocortex, and hippocampus. *Brain Research. Molecular Brain Research*, *48*(2), 259–269. https://doi.org/10.1016/S0169-328X(97)00102-2

Khammy, M. M., Dalsgaard, T., Larsen, P. H., Christoffersen, C. T., Clausen, D., Rasmussen, L. K., Folkersen, L., Grunnet, M., Kehler, J., Aalkjær, C., & Nielsen, J. (2017). PDE1A inhibition elicits cGMP-dependent relaxation of rat mesenteric arteries. *British Journal of Pharmacology*, *174*(22), 4186–4198. https://doi.org/10.1111/bph.14034

Kirstein, M., Rivet-Bastide, M., Hatem, S., Bénardeau, A., Mercadier, J. J., & Fischmeister, R. (1995). Nitric oxide regulates the calcium current in isolated human atrial myocytes. *The Journal of Clinical Investigation*, *95*(2), 794–802. https://doi.org/10.1172/JCI117729

Kitagawa, Y., Hirano, T., & Kawaguchi, S. Y. (2009). Prediction and validation of a mechanism to control the threshold for inhibitory synaptic plasticity. *Molecular Systems Biology*, *5*, 280. https://doi.org/10.1038/msb.2009.39

Klarenbeek, J., Goedhart, J., van Batenburg, A., Groenewald, D., & Jalink, K. (2015). Fourth-generation Epac-based FRET sensors for cAMP feature exceptional brightness, photostability and dynamic range: Characterization of dedicated sensors for FLIM, for ratiometry and with high affinity. *PLoS ONE*, *10*(4), e0122513. https://doi.org/10.1371/journal.pone.0122513

Komas, N., Lugnier, C., & Stoclet, J. C. (1991). Endothelium-dependent and independent relaxation of the rat aorta by cyclic nucleotide phosphodiesterase inhibitors. *British Journal of Pharmacology*, *104*(2), 495–503. https://doi.org/10.1111/j.1476-5381.1991.tb12457.x

Kondabolu, K., Roberts, E. A., Bucklin, M., McCarthy, M. M., Kopell, N., & Han, X. (2016). Striatal cholinergic interneurons generate beta and gamma oscillations in the corticostriatal circuit and produce motor deficits. *Proceedings of the National Academy of Sciences of the United States of America*, *113*(22), E3159–E3168. https://doi.org/10.1073/pnas.1605658113

Krok, A. C., Maltese, M., Mistry, P., Miao, X., Li, Y., & Tritsch, N. X. (2023). Intrinsic dopamine and acetylcholine dynamics in the striatum of mice. *Nature*, *621*(7979), 543–549. https://doi.org/10.1038/s41586-023-05995-9

Lakics, V., Karran, E. H., & Boess, F. G. (2010). Quantitative comparison of phosphodiesterase mRNA distribution in human brain and peripheral tissues. *Neuropharmacology*, *59*(6), 367–374. https://doi.org/10.1016/j.neuropharm.2010.05.004

Lilley, E., Stanford, S. C., Kendall, D. E., Alexander, S. P. H., Cirino, G., Docherty, J. R., George, C. H., Insel, P. A., Izzo, A. A., Ji, Y., Panettieri, R. A., Sobey, C. G., Stefanska, B., Stephens, G., Teixeira, M. M., & Ahluwalia, A. (2020). ARRIVE 2.0 and the British Journal of Pharmacology: Updated guidance for 2020. *British Journal of Pharmacology*, *177*, 3611–3616. https://doi.org/10.1111/bph.15178

Lin, D. T., Fretier, P., Jiang, C., & Vincent, S. R. (2010). Nitric oxide signaling via cGMP-stimulated phosphodiesterase in striatal neurons. *Synapse*, *64*(6), 460–466. https://doi.org/10.1002/syn.20750

Mallet, N., Leblois, A., Maurice, N., & Beurrier, C. (2019). Striatal cholinergic interneurons: How to elucidate their function in health and disease. *Frontiers in Pharmacology*, *10*, 1488. https://doi.org/10.3389/fphar.2019.01488

Matsuoka, I., Suzuki, Y., Defer, N., Nakanishi, H., & Hanoune, J. (1997). Differential expression of type I, II, and V adenylyl cyclase gene in the postnatal developing rat brain. *Journal of Neurochemistry*, *68*(2), 498–506. https://doi.org/10.1046/j.1471-4159.1997.68020498.x

Maurice, D. H. (2005). Cyclic nucleotide phosphodiesterase-mediated integration of cGMP and cAMP signaling in cells of the cardiovascular system. *Frontiers in Bioscience*, *10*, 1221–1228. https://doi.org/10.2741/1614

Maurice, D. H., & Haslam, R. J. (1990). Molecular basis of the synergistic inhibition of platelet function by nitrovasodilators and activators of adenylate cyclase: Inhibition of cyclic AMP breakdown by cyclic GMP. *Molecular Pharmacology*, *37*(5), 671–681.

Maurice, N., Liberge, M., Jaouen, F., Ztaou, S., Hanini, M., Camon, J., Deisseroth, K., Amalric, M., Kerkerian-le Goff, L., & Beurrier, C. (2015). Striatal cholinergic interneurons control motor behavior and basal ganglia function in experimental parkinsonism. *Cell Reports*, *13*(4), 657–666. https://doi.org/10.1016/j.celrep.2015.09.034

Méry, P. F., Pavoine, C., Belhassen, L., Pecker, F., & Fischmeister, R. (1993). Nitric oxide regulates cardiac Ca2+ current. Involvement of cGMP-inhibited and cGMP-stimulated phosphodiesterases through guanylyl cyclase activation. *The Journal of Biological Chemistry*, *268*(35), 26286–26295. https://doi.org/10.1016/S0021-9258(19)74313-0

Mitrano, D. A., & Smith, Y. (2007). Comparative analysis of the subcellular and subsynaptic localization of mGluR1a and mGluR5 metabotropic glutamate receptors in the shell and core of the nucleus accumbens in rat and monkey. *The Journal of Comparative Neurology*, *500*(4), 788–806. https://doi.org/10.1002/cne.21214

Mota, É., Bompierre, S., Betolngar, D., Castro, L. R. V., & Vincent, P. (2021). Pivotal role of phosphodiesterase 10A in the integration of dopamine signals in mice striatal D_1 and D_2 medium-sized spiny neurones. *British Journal of Pharmacology*, *178*(24), 4873–4890. https://doi.org/10.1111/bph.15664

Movsesian, M., Wever-Pinzon, O., & Vandeput, F. (2011). PDE3 inhibition in dilated cardiomyopathy. *Current Opinion in Pharmacology*, *11*(6), 707–713. https://doi.org/10.1016/j.coph.2011.09.001

Muntean, B. S., Dao, M. T., & Martemyanov, K. A. (2019). Allostatic changes in the cAMP system drive opioid-induced adaptation in striatal dopamine signaling. *Cell Reports*, *29*(4), 946–960.e2. https://doi.org/10.1016/j.celrep.2019.09.034

Muntean, B. S., Zucca, S., MacMullen, C. M., Dao, M. T., Johnston, C., Iwamoto, H., Blakely, R. D., Davis, R. L., & Martemyanov, K. A. (2018). Interrogating the spatiotemporal landscape of neuromodulatory GPCR signaling by real-time imaging of cAMP in intact neurons and circuits. *Cell Reports*, *22*(1), 255–268. https://doi.org/10.1016/j.celrep.2017.12.022

Neves, S. R., Tsokas, P., Sarkar, A., Grace, E. A., Rangamani, P., Taubenfeld, S. M., Alberini, C. M., Schaff, J. C., Blitzer, R. D., Moraru, I. I., & Iyengar, R. (2008). Cell shape and negative links in regulatory motifs together control spatial information flow in signaling networks. *Cell*, *133*(4), 666–680. https://doi.org/10.1016/j.cell.2008.04.025

Notomi, T., & Shigemoto, R. (2004). Immunohistochemical localization of Ih channel subunits, HCN1-4, in the rat brain. *The Journal of Comparative Neurology*, *471*(3), 241–276. https://doi.org/10.1002/cne.11039

Padovan-Neto, F. E., & West, A. R. (2017). Regulation of striatal neuron activity by cyclic nucleotide signaling and phosphodiesterase inhibition: Implications for the treatment of Parkinson's disease. *Advances in Neurobiology*, *17*, 257–283. https://doi.org/10.1007/978-3-319-58811-7_10

Percie du Sert, N., Hurst, V., Ahluwalia, A., Alam, S., Avey, M. T., Baker, M., Browne, W. J., Clark, A., Cuthill, I. C., Dirnagl, U., Emerson, M., Garner, P., Holgate, S. T., Howells, D. W., Karp, N. A., Lazic, S. E., Lidster, K., MacCallum, C. J., Macleod, M., … Würbel, H. (2020). The ARRIVE guidelines 2.0: updated guidelines for reporting animal research. *PLoS Biol*, *18*, e3000410. https://doi.org/10.1371/journal.pbio.3000410

Pisani, A., Bonsi, P., Centonze, D., Martorana, A., Fusco, F., Sancesario, G., de Persis, C., Bernardi, G., & Calabresi, P. (2003). Activation of beta1-adrenoceptors excites striatal cholinergic interneurons through a cAMP-dependent, protein kinase-independent pathway. *The Journal of Neuroscience*, *23*(12), 5272–5282. https://doi.org/10.1523/JNEUROSCI.23-12-05272.2003

Polito, M., Guiot, E., Gangarossa, G., Longueville, S., Doulazmi, M., Valjent, E., Hervé, D., Girault, J. A., Paupardin-Tritsch, D., Castro, L. R. V., & Vincent, P. (2015). Selective effects of PDE10A inhibitors on striatopallidal neurons require phosphatase inhibition by DARPP-32. *eNeuro*, *2*(4), ENEURO.0060-15.2015. https://doi.org/10.1523/ENEURO.0060-15.2015

Polito, M., Klarenbeek, J., Jalink, K., Paupardin-Tritsch, D., Vincent, P., & Castro, L. R. (2013). The NO/cGMP pathway inhibits transient cAMP signals through the activation of PDE2 in striatal neurons. *Frontiers in Cellular Neuroscience*, *7*, 211. https://doi.org/10.3389/fncel.2013.00211

Polito, M., Vincent, P., & Guiot, E. (2014). In J. Zhang (Ed.), *Biosensor imaging in brain slice preparations* (Vol. 1071) (pp. 175–194). Humana Press. https://doi.org/10.1007/978-1-62703-622-1_14

Polli, J. W., & Kincaid, R. L. (1994). Expression of a calmodulin-dependent phosphodiesterase isoform (PDE1B1) correlates with brain regions having extensive dopaminergic innervation. *The Journal of Neuroscience*, *14*(3 Pt 1), 1251–1261. https://doi.org/10.1523/JNEUROSCI.14-03-01251.1994

Poppe, H., Rybalkin, S. D., Rehmann, H., Hinds, T. R., Tang, X. B., Christensen, A. E., Schwede, F., Genieser, H. G., Bos, J. L., Doskeland, S. O., Beavo, J. A., & Butt, E. (2008). Cyclic nucleotide analogs as probes of signaling pathways. *Nature Methods*, *5*(4), 277–278. https://doi.org/10.1038/nmeth0408-277

Reinhardt, R. R., & Bondy, C. A. (1996). Differential cellular pattern of gene expression for two distinct cGMP-inhibited cyclic nucleotide phosphodiesterases in developing and mature rat brain. *Neuroscience*, *72*(2), 567–578. https://doi.org/10.1016/0306-4522(95)00520-X

Sano, H., Nagai, Y., Miyakawa, T., Shigemoto, R., & Yokoi, M. (2008). Increased social interaction in mice deficient of the striatal medium spiny neuron-specific phosphodiesterase 10A2. *Journal of Neurochemistry*, *105*(2), 546–556. https://doi.org/10.1111/j.1471-4159.2007.05152.x

Santoro, B., Chen, S., Luthi, A., Pavlidis, P., Shumyatsky, G. P., Tibbs, G. R., & Siegelbaum, S. A. (2000). Molecular and functional heterogeneity of hyperpolarization-activated pacemaker channels in the

mouse CNS. *The Journal of Neuroscience*, *20*(14), 5264–5275. https://doi.org/10.1523/JNEUROSCI.20-14-05264.2000

Saunders, A., Macosko, E. Z., Wysoker, A., Goldman, M., Krienen, F. M., de Rivera, H., Bien, E., Baum, M., Bortolin, L., Wang, S., Goeva, A., Nemesh, J., Kamitaki, N., Brumbaugh, S., Kulp, D., & McCarroll, S. A. (2018). Molecular diversity and specializations among the cells of the adult mouse brain. *Cell*, *174*(4), 1015–1030.e16. https://doi.org/10.1016/j.cell.2018.07.028

Shakur, Y., Holst, L. S., Landstrom, T. R., Movsesian, M., Degerman, E., & Manganiello, V. (2001). Regulation and function of the cyclic nucleotide phosphodiesterase (PDE3) gene family. *Progress in Nucleic Acid Research and Molecular Biology*, *66*, 241–277.

Stocco, A. (2012). Acetylcholine-based entropy in response selection: A model of how striatal interneurons modulate exploration, exploitation, and response variability in decision-making. *Frontiers in Neuroscience*, *6*, 18. https://doi.org/10.3389/fnins.2012.00018

Sudo, T., Tachibana, K., Toga, K., Tochizawa, S., Inoue, Y., Kimura, Y., & Hidaka, H. (2000). Potent effects of novel anti-platelet aggregatory cilostamide analogues on recombinant cyclic nucleotide phosphodiesterase isozyme activity. *Biochemical Pharmacology*, *59*(4), 347–356. https://doi.org/10.1016/S0006-2952(99)00346-9

Tallaksen-Greene, S. J., Kaatz, K. W., Romano, C., & Albin, R. L. (1998). Localization of mGluR1a-like immunoreactivity and mGluR5-like immunoreactivity in identified populations of striatal neurons. *Brain Research*, *780*(2), 210–217. https://doi.org/10.1016/S0006-8993(97)01141-4

Tepper, J. M., Koós, T., Ibanez-Sandoval, O., Tecuapetla, F., Faust, T. W., & Assous, M. (2018). Heterogeneity and diversity of striatal GABAergic interneurons: Update 2018. *Frontiers in Neuroanatomy*, *12*, 91. https://doi.org/10.3389/fnana.2018.00091

Tepper, J. M., Tecuapetla, F., Koos, T., & Ibanez-Sandoval, O. (2010). Heterogeneity and diversity of striatal GABAergic interneurons. *Frontiers in Neuroanatomy*, *4*, 150. https://doi.org/10.3389/fnana.2010.00150

Thestrup, T., Litzlbauer, J., Bartholomaus, I., Mues, M., Russo, L., Dana, H., Kovalchuk, Y., Liang, Y., Kalamakis, G., Laukat, Y., & Becker, S. (2014). Optimized ratiometric calcium sensors for functional in vivo imaging of neurons and T lymphocytes. *Nature Methods*, *11*(2), 175–182. https://doi.org/10.1038/nmeth.2773

Vandecasteele, G., Verde, I., Rucker-Martin, C., Donzeau-Gouge, P., & Fischmeister, R. (2001). Cyclic GMP regulation of the L-type ca(2+) channel current in human atrial myocytes. *The Journal of Physiology*, *533*(Pt 2), 329–340. https://doi.org/10.1111/j.1469-7793.2001.0329a.x

Wennogle, L. P., Hoxie, H., Peng, Y., & Hendrick, J. P. (2017). Phosphodiesterase 1: A unique drug target for degenerative diseases and cognitive dysfunction. *Advances in Neurobiology*, *17*, 349–384. https://doi.org/10.1007/978-3-319-58811-7_13

West, A. R., Galloway, M. P., & Grace, A. A. (2002). Regulation of striatal dopamine neurotransmission by nitric oxide: Effector pathways and signaling mechanisms. *Synapse*, *44*(4), 227–245. https://doi.org/10.1002/syn.10076

West, A. R., & Grace, A. A. (2000). Striatal nitric oxide signaling regulates the neuronal activity of midbrain dopamine neurons in vivo. *Journal of Neurophysiology*, *83*(4), 1796–1808. https://doi.org/10.1152/jn.2000.83.4.1796

West, A. R., & Tseng, K. Y. (2011). Nitric oxide-soluble guanylyl cyclase-cyclic GMP signaling in the striatum: New targets for the treatment of Parkinson's disease? *Frontiers in Systems Neuroscience*, *5*, 55. https://doi.org/10.3389/fnsys.2011.00055

Xie, Z., Adamowicz, W. O., Eldred, W. D., Jakowski, A. B., Kleiman, R. J., Morton, D. G., Stephenson, D. T., Strick, C. A., Williams, R. D., & Menniti, F. S. (2006). Cellular and subcellular localization of PDE10A, a striatum-enriched phosphodiesterase. *Neuroscience*, *139*(2), 597–607. https://doi.org/10.1016/j.neuroscience.2005.12.042

Zemskov, E. A., Wu, X., Aggarwal, S., Yegambaram, M., Gross, C., Lu, Q., Wang, H., Tang, H., Wang, T., & Black, S. M. (2021). Nitration of protein kinase G-Iα modulates cyclic nucleotide crosstalk via phosphodiesterase 3A: Implications for acute lung injury. *The Journal of Biological Chemistry*, *297*(2), 100946. https://doi.org/10.1016/j.jbc.2021.100946

Zhao, Z., Zhang, K., Liu, X., Yan, H., Ma, X., Zhang, S., Zheng, J., Wang, L., & Wei, X. (2016). Involvement of HCN Channel in muscarinic inhibitory action on tonic firing of dorsolateral striatal cholinergic interneurons. *Frontiers in Cellular Neuroscience*, *10*, 71. https://doi.org/10.3389/fncel.2016.00071

Ztaou, S., Maurice, N., Camon, J., Guiraudie-Capraz, G., Kerkerian-Le Goff, L., Beurrier, C., Liberge, M., & Amalric, M. (2016). Involvement of striatal cholinergic interneurons and M1 and M4 muscarinic receptors in motor symptoms of Parkinson's disease. *The Journal of Neuroscience*, *36*(35), 9161–9172. https://doi.org/10.1523/JNEUROSCI.0873-16.2016

How to cite this article: Bompierre, S., Byelyayeva, Y., Mota, E., Lefevre, M., Pumo, A., Kehler, J., Castro, L. R. V., & Vincent, P. (2024). Cross-pathway integration of cAMP signals through cGMP and calcium-regulated phosphodiesterases in mouse striatal cholinergic interneurons. *British Journal of Pharmacology*, 1–18. https://doi.org/10.1111/bph.17400